UNIVERSITY OF SOUTHERN QUEENSLAND

FACULTY OF HEALTH, ENGINEERING & SCIENCES

A Numerical Investigation into Sinkhole Formation

A DISSERTATION SUBMITTED BY

Anthony James Keightley

U1019495

IN FULFILMENT OF THE REQUIREMENTS OF

ENG4111 / ENG4112 Research Project

towards the degree of

BACHELOR OF ENGINEERING (Honours-CIVIL)

05/01/16

Abstract

Sinkholes pose danger to the environment through the associated gradual subsidence or sudden collapse of the ground that can lead to loss of lives and damage to property. Sinkholes develop in different sizes, shapes and rates all over the world. This project assists in further understanding how sinkhole development can be analysed through analytical theories and the application of numerical methods to create simulations. It involves the investigation, development and verification of numerical models aimed at determining the slope stability of differing trapdoor scenarios. The analysis will be completed through using the computer program Fast Lagrangian Analysis of Continua (FLAC). The completion of 2D numerical models gives the chance to simulate many different sinkholes, with varying material properties and different overburden depth to cavity width and length ratios.

Sinkholes are analysed by strength reduction method, producing the factor of safety of the overburden above a trapdoor. The numerical study appraised sinkhole propagation with the Fast Lagrangian Analysis of Continua software to determine the slope stability of differing trapdoor scenarios. This furthered the understanding of sinkhole mechanics by providing a more realistic model in relation to an actual sinkhole formation. The extent of surface failure was investigated and found to be dependent upon the depth ratio of the sinkholes trapdoor.

The many varying cases with regards to surcharge pressure and internal pressure within the cavity where tested to determine to what extent the pressure ratio affected the resulting sinkhole formed under these varying pressure conditions. Scenarios were initially tested with zero pressure ratios and then rerun with both positive and negative pressure ratios to simulate both collapse failure as well as blowout of the sinkhole.

Stability Charts were developed for both the zero pressure ratio and non-zero pressure ratio scenarios and possible practical applications demonstrated to allow for quick ascertainment of conditions and the associated factor of safety or critical conditions.

University of Southern Queensland

Faculty of Health, Engineering and Sciences

ENG4111/2 Research Project

Limitations of Use

The Council of the University of Southern Queensland, its Faculty of Health, Engineering & Sciences, and the staff of the University of Southern Queensland, do not accept any responsibility for the truth, accuracy or completeness of material contained within or associated with this dissertation.

Persons using all or any part of this material do so at their own risk, and not at the risk of the Council of the University of Southern Queensland, its Faculty of Health, Engineering & Sciences or the staff of the University of Southern Queensland.

This dissertation reports an educational exercise and has no purpose or validity beyond this exercise. The sole purpose of the course pair entitled "Research Project" is to contribute to the overall education within the student's chosen degree program. This document, the associated hardware, software, drawings, and other material set out in the associated appendices should not be used for any other purpose: if they are so used, it is entirely at the risk of the user.

Certification of Dissertation

I certify that the ideas, designs and experimental work, results, analyses and conclusions set out in this dissertation are entirely my own effort, except where otherwise indicated and acknowledged.

I further certify that the work is original and has not been previously submitted for assessment in any other course or institution, except where specifically stated.

Anthony James Keightley

Student Number:

_____

Signature

_____

Date

Acknowledgements

I would like to acknowledge the support and assistance that I have received throughout the development and research of this project. In particular I would acknowledge my family and friends, for their support, tolerance and encouragement throughout the entire process of this project. I would like to thank my supervisor Dr Jim Shiau who has been helpful in providing guidance and technical support along with the Tunnelling Research Group with respect to the development of the FISH code utilised.

Special thanks to Brian Lamb and Matthew Sams for their guidance and influence towards the project.

Anthony James Keightley

University of Southern Queensland

Contents

List of Figures

List of Tables

Nomenclature

c	Cohesion (Pa)
c_u	Undrained shear strength (Pa)
FOS	Factor of Safety
FLAC	Fast Lagrangian Analysis of Continua
γ	Soil self-weight kN/m^3
H	Depth of overburden (m)
N	Pressure Ratio
N_c	Critical Pressure Ratio
S_u	Undrained shear strength (Pa)
SR	Strength Ratio
$(SR)_c$	Critical Strength Ratio
SSR	Shear Strain Rate
σ_s	Surcharge
σ_t	Internal Pressure
W	Trapdoor Cavity Width (m)

Chapter 1

Introduction

This theis is focused on investigating sinkholes through research and 2D modelling. By applying previously learnt civil and geotechnical engineer knowledge and researching into previous sinkhole collapses and relevant literature the investigation will continue on from a previous investigation by Lamb (2014). The generation of idealised 2D models describing the sinkhole phenomena adds to the current body of knowledge for sinkhole mechanics. This paper focuses on the trap door method for sinkhole simulation as a new technique which allows for relevant numerical data to be collected making a positive contribution to sinkhole research. Fast Lagrangian Analysis of Continua (FLAC) software produced by the Itasca Consulting Group, Inc. is used for the 2D analysis.

This chapter provides an overview of this modelling. The topics addressed include the background, project scope and objectives, a methodology summary, project contributions and an outline of the dissertation.

1.1 Background

“Sinkholes are depressions or shafts formed at a soil surface due to changes in the soil and or rock beneath. In limestone areas the gradual erosion of rock at a depth caused by the passing of underground water leads to subsidence of the overburden of the remaining and deposited soil and a resulting saucer-shaped depression.”(Sowers 1996)

Occurring around the globe sinkholes not only can cause devastating consequences but also contribute to the endless change that shapes and reshapes the world. Despite their volatility, sinkholes form due to a somewhat predictable combination of geology and weather. A sinkhole mainly forms in karst landscapes by erosion of

the sedimentary terrain creating a hole or depression viewable on the ground surface.

Whether they have formed gradually or suddenly, natural and human-caused sinkholes have swallowed up land, cars, people and houses around the world. They have become phenomena which are of high interest to scientists and the public due to the nature of how they suddenly occur. As previously mentioned, naturally occurring sinkholes mainly form in karst landscapes but they can happen anywhere with soluble subsurface rock. Well-known cases are the Qattara Depression in Egypt which is roughly 80km by 121km in surface size and is one of the largest natural sinkholes in the world; and The Great Blue Hole off the coast of Belize is an example of an underwater sinkhole.

Sinkholes are predominantly of two main types, cover-collapse sinkholes, which can develop abruptly and cover-subsidence sinkholes, which form slowly over time with the ground gradually sinking or collapsing. Sinkhole collapses can range in size and severity.

Differing circumstances result in collapse but are all based on the overburden soil pressures increasing to breaking point where the overburden material collapses. Overburden can be seen as the material either natural or manmade structures above an underground cavity. The inevitable collapse of the overburden into the underground cavity leaves in most cases, an inverted conical shape and circular ground opening.

The resulting surface appearance of the sinkhole appears to be influenced by the cavity roof aspect ratio. It can be assumed that the resulting surface opening will be circular if the aspect ratio is approximately 1:1. (Lamb 2014)

Sinkholes can occur due to the interference of manmade constructions or excavations caused by the weakening of the earth through mining, construction, and the manipulation of ground and surface water. Causes also occur naturally due to the geotechnical characteristics, often at the rock-soil interface due to the

dissolution of strata below the soil. Changing weather patterns furthermore affect the rate of formation of sinkholes due to these varying conditions.

There have been numerous attempts to produce models of sinkhole collapse, to aid in producing an increased understanding of the mechanics of collapse. These include graphical information systems (GIS) as explained in (Marini n.d) and (Neubert 2008). Finite-element limit analysis techniques have successfully modelled a sinkhole for its un-safe surcharge limit with a spherical underground cavity as shown in Augarde et al. (2003).

This thesis offers a continuation of the trapdoor method of modelling sinkhole overburden stability. This method uses the strength reduction method to find the stability of a sinkhole case with reference to its factor of safety caused due to its self-weight (γ).

1.2 Methodology

The methodology for this paper is as follows:

i. Research literature relevant to sinkholes, stability and sinkhole simulations.

ii. Complete a literature review of relevant material on this topic.

iii. Complete a case study of past sinkhole collapses.

iv. Study the background and learn how to use FLAC to analyse sinkholes for factor of safety and how to produce valuable outputs.

v. Carry out cases across their different materials for 2D analysis investigating undrained clay

vi. Analysis the Pressure ratios (N) = 0 results obtained from the 2D analysis.

vii. Carrying out cases to achieve results where Pressure ratios (N) ≠ 0

viii. Analysis the Pressure ratios (N) ≠ 0 results obtained

ix. Discuss how the simulations and results can increase the understanding of sinkhole formation and have a positive impact.

1.3 Research Objectives

The main objective of this project is to reiterate on the fundamental knowledge of sinkholes and their formations and also to provide further advancement in knowledge of the sinkhole phenomena. Determining the possibility of collapse will be attempted by strengthening of overburdening soil and factor of safety calculations to be completed. Investigation of the effect of pressure ratios on the eventual failure of sinkhole models in a two dimensional context. The results gathered will be compared against previous works to ensure reliability and also feasibly increase the understanding of soil stability over cavity openings.

1.4 Project Contributions and Consequential Effect

The contribution of this project to the literature in the development of sinkhole understanding and modelling is the refinement of 2D numerical models of overburden collapse with varying cavity roof depths and extended to include varying pressure ratios. The material that was studied in this parametric study was purely cohesive homogenous undrained clay. The shear stress rates provide a measure of the deformation and plasticity of the overburden collapse due to the opening of the trapdoor. The principal of soil arching over trapdoors was investigated and the factor of safety of sinkhole overburden was calculated as a practical method for finding a stability solution to potential overburden collapses.

1.5 Organisation of Thesis

Chapter 2 – General Review: This section of the report defines the background behind sinkholes, including the formation, cause and collapse mechanics as expressed in current relevant literature, incorporating a section on both naturally created and human created sinkholes. A review of current sinkhole numerical models, are studied with an insight into the prediction of formation, triggering mechanisms and influential factors of specific ground failures and sinkhole events. The factor of safety is discussed, as well as, a review of case studies with the view of presenting the effects of real life sinkhole collapse have been included. Finally the stability of trapdoors is discussed.

Chapter 3 – Numerical Modelling and FLAC Methodology: discusses the uses of FLAC Software as a modelling tool, its advantages, disadvantages and the reasoning behind why FLAC was chosen to be used. Also the strength reduction method FLAC uses to calculate the factor of safety (FOS) of the sinkhole cases is explained. The FLAC user manual is utilized as the main source of information in this chapter to summarise the relevant mechanics behind the software package.

Chapter 4 – Analysis of Underground Trapdoors with zero Pressure Ratio: This chapter introduces the 2D numerical analysis to the sinkhole trapdoor method. Two dimensional analyses of underground trapdoors with zero pressure ratios will be investigated. The analysis of these ratios is done with a variation of the depth or height of soil overburden (H), while keeping a constant fixed width of cavity opening (W) to simplify the task. Shear strain rates, effective stresses, displacement and plasticity indicators are analysed and discussed here. The creation of a factor of safety function dependant on both the strength and depth ratio has been proposed. This function is linked to the creation of stability charts.

Chapter 5 - Analysis of Underground Trapdoors with Varying Pressure Ratio: In this chapter, FLAC 2D will be used to analysis of underground trapdoors with the introduction of varying non-zero pressure. The analysis of these ratios is done with a variation of the depth or height of soil overburden (H), while keeping constant

fixed width of cavity opening (W) to simplify the task. In the software modelling only half the cavity width is simulated to reduce calculation times. The investigation of the non-zero pressure ratios has led to the introduction blowout failures and the determination of possible maximum stability conditions resulting in equilibrium scenarios.

Chapter 6 – Conclusions: The final chapter summarises all the findings of the study as well as discussing the key outcomes. A statement of future recommendations for continued work on the topic will present in this section.

Chapter 2

Background and Literature Review

This section of the report defines the background behind sinkholes, including the formation, cause and collapse mechanics as expressed in current relevant literature. It is understood that "Sinkholes result from the differential lowering of the surface by dissolution or from a combination of subsurface dissolution processes and internal erosion and deformation processes (subsidence) affecting the overlying material." *(*Gutiérrez *2006).* Subsidence and sinkhole events may occur gradually or abruptly.

The natural process of water gradually dissolving small parts of the rock, enlarging its natural fissures and joints and creating cavities beneath the earth, cause changes to soil. As the process continues, loose unconsolidated soil and sand above is gradually washed into these cracks and voids. Depending on how thick and strong that top layer is and how close to the surface the void beneath is, the land may not be able to sustain its own weight – and that of whatever we build on top of it. The surface layer will simply give way, creating a funnel-shaped depression, with a hole at the centre, this being a sinkhole.

Most natural sinkholes form in the soft layer of underground rock. The ground above it and on the surface is called the overburden which can vary in depth, depending on the depth of the upper most part of the cavity. The overburden's material properties have a great effect on the dependence of a collapse. The process of the overburden collapsing into the cavity, creating a sinkhole is referred to as failure. Failure is also the process of dynamic subsidence occurring over time within the overburden before a collapse. The size of these sinkholes depends upon the thickness and bearing properties of the overburden sediments.

To study and understand the characteristics of sinkhole collapse, relevant literature was gathered and reviewed. Numerical models were generated with the overburden being homogeneous undrained material with varying strength ratios

and cavity depths for each. The undrained clay was also tested under the effects of varying pressure ratios.

The method to examine the sinkhole stability numerically is to calculate the factor of safety (FoS) of each case for a trapdoor scenario. The trapdoor scenario is that the soil overburden is set at equilibrium and then a portion underneath the overburden is spontaneously released. This causes the overburden to collapse due to its self-weight.

2.1 Collapse Mechanics

The mechanism of subsidence can help define a sinkhole. To put things into perspective, we can refer to the definition, "A sinkhole can be defined as a subsidence feature that can form rapidly and that is characterized by a distinct break in the land surface and the downward movement of surface materials into the resulting hole or cavity." (Mining 2006) The collapse feature is a result of soil or related materials being transported down into the void.

Mechanisms that initiate most natural and induced sinkholes are the same. Assessment of existing or potential sinkhole problems at a site requires recognition of features associated with sinkhole development and knowledge of triggering mechanisms that cause sinkholes. Warren (1974)suggests that three things need to be present in order for subsidence and/or collapse of sinkholes to occur – 1) there must be an outlet in the underlying bedrock; 2) the soil must be detachable or movable; and 3) there must be a driving mechanism. (Manger et al. 1986) Specific examples of driving mechanisms include surface drainage modifications, land disturbances, and water table alterations.

The overburden is subjected to stress, strain and shear forces as explained in 'Potential Impacts of underground Mining' (Mining 2006). These lead to subsidence ground movements that are both horizontal and vertical in nature. The shear force due to the overburden weight causes a maximum vertical movement at the centre

of the subsidence that gradually reduces until the boundary, where no surface deformation is reached.

The initial vertical movement of the overburdening soil causes horizontal movement to fill the void created by the vertical movement of the overburden. This movement causes compressive strains at the surface. These compressive strains are greatest at the centre of the subsidence and become less the further from this central point. Past this point the stresses become tensile due to adjacent points are horizontally further apart. At this point of equilibrium, the inflection point, the surface of subsidence changes from convex to concave.

These regions of compressive and tensile forces represented as strains due to the linear deformation of the surface overburden compared to its original placement. The inner section of subsidence undergoes compressive strains directly about the centre of failure and is known as the compressive zone. The tensile zone is the zone that often extends beyond the cavity failure. This paper will focus on the failure of the overburden due to compressive properties of the soils and their friction angles. This is because soil has little or no tension capabilities.

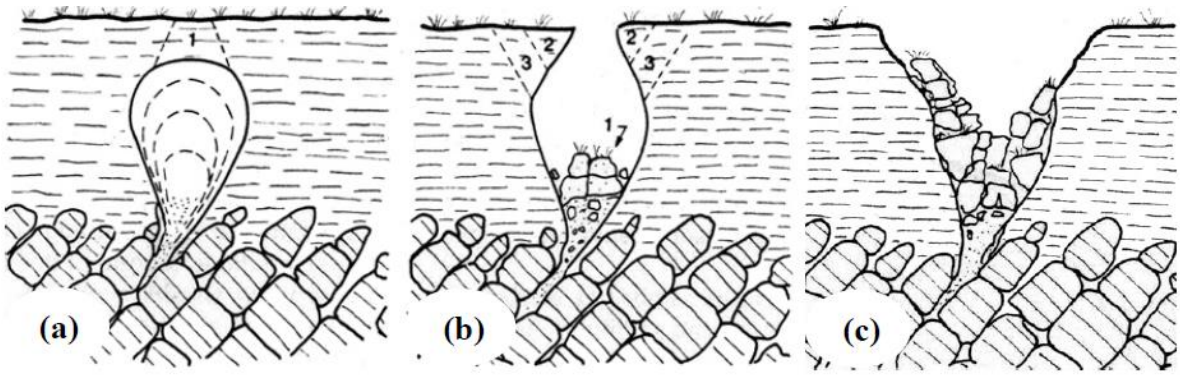

Figure 1 - Sinkhole Collapse (Sowers 1996)

As seen in Figure 1, the resulting shape of the collapsed overburden is generally conical. This outcome occurs when the strain is greater than the required stability conditions of the overburden and the soil pressure distribution no longer is able to self-support itself.

Generally, the cavity enlarges outward and upward towards the ground surface. In cases where a source of infiltration exists, such as a leaking pipe, the upward propagation of the cavity will deviate toward that source. The shape of the cavity varies with the nature of the overburden layer, where wider cavities are more likely to develop in more cohesive soils.

2.2 Causes of Failure

2.2.1 Naturally created Sinkholes

Naturally occurring sinkholes are most common in limestone rock and salt beds that are easily dissolved by moving water. They are the result of the chemical weathering of carbonate rocks like limestone, the type of landscape made up of these rocks is known as karst topography. As stated by Sinkhole Formation Mechanism (Baryakh 2001), a karst process can develop in the following stages: (1) formation of a cavity; (2) growth of the cavity under leaching; (3) reaching of ultimate dimension; (4) collapse of overlying rocks into the cavity (plastic and granular rocks), further growth of the cavity and the associated deformation of the earth surface; (5) gradual fill of the cavity with rocks and formation of a sinkhole on the earth surface.

Tectonic actions are another natural cause of sinkholes formation. Crustal movements including extension, cooling and loading disrupts its structure, creating points of weakness allowing areas of karst topography to develop.

In the case of soluble rocks, sinkhole development depends on limestone dissolution, water movement, and other environmental conditions. Limestone dissolution rates (on the order of millimetres per thousand years) are highest in areas where precipitation rates are high. Cavities develop in limestone over geologic time and result from chemical and mechanical erosion of material (Ford 1989).

In the case of insoluble rocks, the underground cavity is developed during the rock formation (Budetta 1995). The sinkhole is created when the roof drops into the

cavity due to weathering and erosion or imposed load, exceeding the load beyond the roof's strength.

Prolonged periods of certain weather conditions, like drought, also affect the water table level which in turn alters the buoyant forces that may be upholding the overburden. This drop in the forces may lead to failure of the cavity roof resulting in the sink hole.

2.2.2 Human created Sinkholes

Satarugsa (2011)suggests a variety of human activities can accelerate or trigger an underground collapse into sinkholes. The major factor is the increased water flow through soil and cavity. This is due to runoff drainage, broken pipes, or unlined ditches which accelerate soil erosion and cavity expansion leading to underground structural failure and sinkholes.

Satarugsa (2011) also suggest that over pumping of bore water from artesian bores can reduce or eliminate the buoyant forces that may be necessary to hold up the overburden above an underground cavity. Other human activities that cause a similar situation are oil drilling and gas extraction, tunnelling and pipelines that may collapse if not engineered effectively.

In terms of construction, compacting soil beneath large structures to eliminate the probable source of underlying cavities may prevent sinkholes from occurring in these sites.

2.3 Current Sinkhole Models

Augarde et al. (2003) predicted the collapse of undrained sinkholes via a submerged spherical cavity method. They note that analytical approaches for the study of sinkholes are surprisingly rare within literature.

Augarde et al. (2003) explains that in the past research has been conducted into the stability of overburden soil through a centrifuge method. These models used an idealised cavity and the collapse of the overburden was caused only by the overburden weight. Overburden weight was gradually increased via increasing the centrifuge speed until the overburden clay collapsed into a cylindrical cavity. They found that the failure into the rigid body cylinder which was the cavity was adequate for the modelling of the sinkhole.

2.4 Prediction of Collapse

Lei (2005) explains that a sinkhole collapse is most often an instantaneous event, making it extremely difficult, taking in situ measurements during the collapse failure. This makes it increasingly difficult to investigate the formation, triggering mechanism and influential factors of specific ground failures and sinkhole events.

Blom (2013) of NASA, have recently analysed interferometric synthetic aperture radar (InSAR) imagery of a region near Bayou Corne, Louisiana and were able to detect indications of a large sinkhole before it collapsed. Their analysis showed significant horizontal ground deformation towards where the sinkhole formed at least a month before the collapse. These horizontal movements were up to 260 mm in size and covered an area 500m by 500m, which was much greater than the initial sinkhole. Blom indicates that their finding do demonstrate one of the benefits of an InSAR satellite that would image wide areas frequently.
(Corne 2014)

Most research regarding the prediction of sinkhole formation is descriptive rather than analytical in nature as explained by Augarde et al. (2003). There no generic research into predicting sinkhole formation as most research is related to local geology or particular sites.

2.5 Trapdoor

Stability of trapdoors has been previously studied. Sloan et al. (1990) studied the undrained stability of a trapdoor. This paper is investigating undrained clay sinkhole which is similar to the previously mentioned model. This paper examines the stability of a purely cohesive soil layer resting on top of a trapdoor. The plane strain trapdoor problem as discussed in this paper is shown in Figure 2. The layer of cohesive soil with undrained shear strength (c_u) is resting on top of the trapdoor with a width (B) and soil thickness (H).

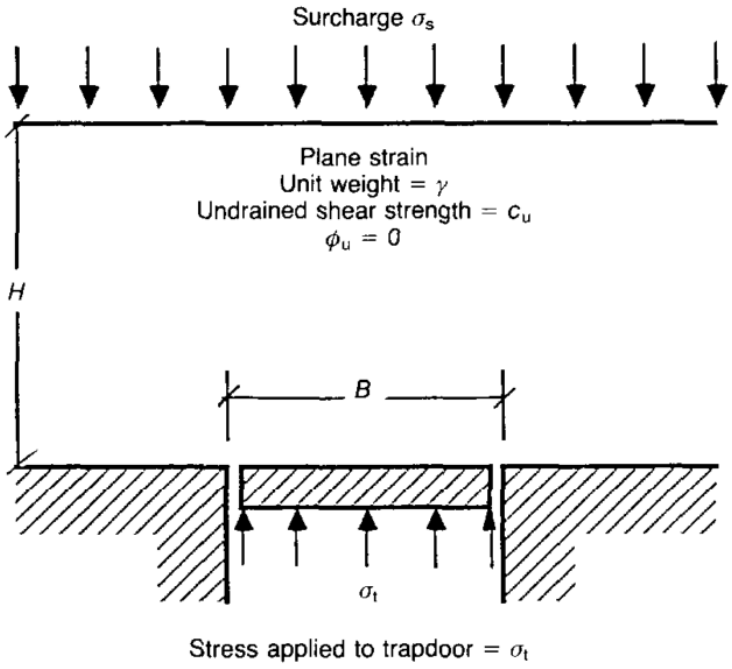

Figure 2 - Trapdoor scenario with surcharge and trapdoor upward pressure (Sloan et al., 1990)

Sloan et al. (1990)showed that the stability of the trapdoor was determined by

$$N = (\gamma H + \sigma_s - \sigma_t)/c_u \qquad (2.1)$$

Sloan states that this stability number (N) is a function of $\frac{H}{B}$ and that it was based theoretically on a factor of safety of 1.Recalling the work of Davis (1980) he demonstrated that the stability number had a lower bound and upper bound that meant $2\log_e\left(\frac{2H}{B}\right) \leq N \leq \frac{2H}{B}$, justifying the dependence of the stability number (N) on the depth to width ratio.

It has also been recalled by Radoslaw L. Michalowski (2002) that the stability number is a function of the factor of safety (F). Using the work of (Taylor 1937) the stability number was initially express in the form

$$N = \frac{c}{\gamma HF} \qquad (2.2)$$

This equation is the reciprocal of equation proposed by Sloan. In Taylors original paper of the 1930's the soil surcharge and trapdoor internal vertical pressure were not considered and therefore $\sigma_s = \sigma_t = 0$ resulting in equation becoming

$$N = (\gamma H)F/c_u \qquad (2.3)$$

given the factor of safety is now included.

However, the process of soil arching is a major effect of the overburden load. The soil arches in an attempt to provide stability from the created stresses in the soil. This is an internal process. By including the upward roof pressure σ_t in the model it may be possible determine the pressure required to maintain stability for a given factor of safety. The results in the model

$$N = (\gamma H - \sigma_t)F/c_u \qquad (2.4)$$

2.6 Factor of safety (FoS)

Factor of safety is the result of the task used to analyse the stability of a given slope. The outcome of a factor of safety (FoS) equal to 1 categorizes the analysed slope to be in a state of impending failure. As stated by Hong Zheng the factor of safety (FoS) can be defined as the factor by which the shear strength of the soil would have to be divided to bring the slope into the state of critical equilibrium.

To determine the factor that is needed to bring the slope to its critical equilibrium, the strength reduction method is applied. To reach the critical equilibrium, the shear strength is reduced gradually. The strength reduction method for determining the factor of safety can now be implemented in FLAC through the use of the SOLVE fos command. When activated, this function will start an automatic search for the factor of safety using a bracketing approach. The materials cohesion and angle of friction are also reduced until equilibrium is achieved and now allows for the calculation of the factor of safety (FoS). In this investigation the angle of friction is set to zero initially and the process is purely a reduction in strength.

The function of the cohesion and the internal friction angle is known as the Mohr-Coulomb yield criterion. Overall the safety of soil structures can reasonably be determined by the calculations of the factor of safety and are an accepted process that is in practice.

The ITASCA software FLAC has the ability to determine the factor of safety for any selected parameter by calculating the ratio of the modelled value under given conditions to that which results in failure. In this investigation the factor of safety is the ratio of the applied load to cause failure to the design load. The definition of failure must be established by the user. (ITASCA ConsultingGroup 2011)

2.7 Strength Reduction Method

The factor of safety (FoS) for a slope may be computed by reducing shear strength of rock or soil in stages until the slope fails. This method is called shear strength reduction technique (SSR). (Cala .M 2004)

The factor of safety (FoS) is traditionally defined as the ratio of the actual soil shear strength to the minimum shear strength required to prevent failure (Bishop 1955). Since it is defined as a shear strength reduction factor, an obvious way of computing FoS with a finite element or finite difference program is simply to reduce the soil shear strength until collapse occurs. The resulting factor of safety is the ratio of the soil's actual shear strength to the reduced shear strength at failure.

Using FLAC (Itasca Consulting Group), the factor of safety is computed using explicit-finite-difference-code. FLAC uses dynamic relaxation (Otter 1966), which is an explicit, time-marching procedure in which the full dynamic equations of motion are integrated step by step. Convergence criteria in FLAC is used at every node in the mesh under investigation and the simulation is said to have converged when all normalised unbalanced force ratios are less than 10^{-3}. If the unbalanced force ratio is greater than 10^{-3}, then further steps are executed.

Advantages of the strength reduction method include:

- not having to define a failure surface or search for a minimum failure surface
- equations of equilibrium are all satisfied
- strains and displacements in the material can be calculated

Disadvantages of the strength reduction method include:

- is a relatively new approach compared to the Limit equilibrium method
- requires more input about soil properties and boundary conditions
- mesh generation and model setup can be difficult
- it can be much slower and compute time intensive

- its restriction to Mohr-Coulomb materials

Recent studies (Cheng et al., 2006) indicate that the strength reduction method is comparable to the more widely accepted Limit Equilibrium Method.

2.8 FISH Programming Language

Within FLAC is a programming language known as FISH that gives the user the ability to define new variables and functions. These functions may be used to enhance the usefulness of FLAC through the use of these user defined features.

The development of FISH language followed user requests to simplify the use of Itasca Software in situations that were difficult or impossible using the existing program structure.

Sometimes FLAC's built-in grid generators will not be able to produce a desired geometry. A series of INITIAL commands can always be used to specify locations of individual grid points if all else fail. This can be tedious if every x- and y-point must be specified individually, but it is often possible to write a program that generates the grid automatically using the built-in programming language, FISH. (Group 2014)

Within this investigation the FISH programming language is utilised to generate the required grid to simulate the geometry and geology of the region surrounding the trapdoor collapse. The FISH script designed as part of this investigation for the Tunnelling research group, of which this thesis is a product. The script sets the soil properties, mesh size and geometry of half a trapdoor scenario and enables the parametric studies to be carried out efficiently.

2.9 Sinkhole Case Studies

2.9.1 China

Zhu Xuewen and Chen Weihai (Weihai n.d) examine sinkholes in the area of China that have the most extensive and diversified karst terrains in the world that are rich in caves and dolines. The area of cone karst and tower karst developed in the humid climate in southern China and form distinctive karst landscapes. Tiankengs, 'sky holes', are giant dolines that are a feature in some areas of the cone karst. There are less than a hundred tiankengs known in the whole world. The trigger effect that caused the collapse of the tiankengs developed through an unusual hydrodynamic combination of erosion, dissolution and collapse. The cave river that is a within the karst is a powerful force in removing material from Xiaozhai Tiankeng. They form by multiple phases of progressive wall and roof breakdown, probably over time spans of a million years or more. They add a dimension to geomorphological concepts of major collapse and perhaps gorge evolution in karst.

In these carbonate rock terrains, a prominent sinkhole, Xiaozhai tiankeng, is recognized as a rare negative karst landform which occurs only in more remote regions of China. With its steep walls and reaching several hundred metres in depth and diameter it may rank as the largest tiankeng in the world. It has an entrance diameter of 537 to 626 m, a depth of 662 m and a volume of 119.35M m3.

Zhu Xuewen and Chen Weihai explain that the Xiaozhai Tiankeng profile has a double nested structure; the upper bowl is 320 m in depth, and the lower shaft is a rectangle 342 m in depth and 257-268 m across; the sloping ledge between these two parts is formed at the level of a muddy limestone. As they form over several phases of progressive wall and roof breakdown, over a million years or more, a tiankeng can be large enough to swallow a small town, but there is no evidence that any could develop suddenly to cause unexpected damage.

2.9.2 America

New Mexico

Sinkholes formed in gypsum bedrock in the Delaware Basin region are of human origin. They are usually associated with improperly cased abandoned oil wells, or with solution mining of salt beds in the shallow subsurface. Located on state trust land ~35 km northeast of Carlsbad, a sinkhole abruptly formed on the morning of July 16th 2008. Lewis Land (Land 2013) provides this example of a man induced sinkhole caused by a Brine Well that was engulfed by the sinkhole along with the surrounding associated structures. Refer to Figure 3. Solution mining was being conducted in the Salado Formation by the Brine Well. This involved injecting and circulating fresh water through the 86 m thick section of halite. This process was continued until saturation was accomplished.

Figure 3 - LWS Sinkhole

The sinkhole was filled with water and measured to be several tens of meters in diameter and had a depth below the ground level of around 12 m. Surrounding the perimeter, large concentric fractures began to advance, towards the nearby road to the south which endangered its integrity.

In just over a week, the water originally present had subsided into the subsurface and the vertical walls of the sinkhole had settled to a bank of around 45 degrees extending to a depth of approximately 20 m.

Lewis Land (Land 2013)states that the water was solution mining fluid that in the initial stages of the collapse had been drawn to the surface through the debris chimney as there were no significant groundwater sources at these shallow depths. The resulting collapse of the subsurface cavern was due to this fluid being stored in pore space. The sinkhole had finally increased to a depth of approximately 45 m and spanned in diameter of close to 111 m.

2.9.3 Mexico

Thought to be the second deepest sinkhole in Mexico is the 'Cave of Swallows, Sótano de las Golondrinas. The association for Mexican Cave Studies explains that it is one of the largest limestone sinkholes in the world known to mankind. (RAINES 1968)

It is further explained that the surface shape of the sinkhole is 49m by 62m wide giving it an elliptical entrance. It becomes much larger at the bottom, measuring 303m by 134m. It is recognized as the largest cave shaft in the world, the greatest depth from the highest side is a 370m freefall drop and a 333m on the adjacent lower side.

The walls of the pit look nearly vertical when looking in from above and the entrance and floor seem to be of equal dimensions. It is not until one has descended several hundred feet that the proper perspective of the pit can be realized.

Evidently, Sotano de las Goloridrinas was formed through the development of a large phreatic room and collapse of ceiling and wall rock. Erosion and mass movements along a major fault line in the lower Cretaceous limestone in the Sierra Huasteca over time have caused the evident enlargement of the cave. The eventual collapse of the roof was due to the inability of the cave walls to support the overburdening material, thus resulting in the open air sinkhole seen today.

2.9.4 Australia

Mount Gambier

The cave garden, Umpherston Sinkhole, is a well-known sinkhole that is located in the city of Mount Gambier. The formation of this sinkhole and the ones that surround the city have become the centre of attraction for tourists even though they are quite dangerous due to their possible future evolution.

The southern coast of South Australia is a region that has a predominant layer of underlying limestone where the sinkholes around the city of Mount Gambier have developed. Dissolved carbon dioxide creates a weak acid and is present in rainwater that falls from the atmosphere. Due to the permeability and high porosity of limestone, it acts as an aquifer and holds this weak acid which slowly dissolves the layer of limestone over time, creating cavities and in turn the beginning of sinkholes.

2.9.5 Central America

Belize

An example of one of the few large, cylindrical submarine reefal karst cavities is the Blue Hole of Belize examined by Gischler (2013). It can be seen that this sinkhole had once been above the water level in a former orientation as it has unusual tilted stalactites at great depths. Past geological shifts and tilting of the underlying plateau can be identified as some of the stalactites were non-vertical and off by around 5 degrees. In certain places the sinkhole can be measured to be 125 m deep and 320 m wide. Coalesced coral patch reefs almost completely surround its cylindrical shape which has left a circular ridge of debris at its floor. The cylindrical shape of the hole presumably results from the collapse of the roof of a karst cave (Dill 1977).

Being one of the largest natural blue hole formations, the Belize Blue Hole provides a high-resolution archive of climates and storms in its undisturbed, annually-layered muddy sediment base. Not only is it believed to be the world's largest ocean-floor sinkholes, it is a virtually unique pleistocene sinkhole.

A summary of these sinkhole case study findings can be found in Appendix B.

Chapter 3

3.1 FLAC Software as a modelling tool

"FLAC is a two-dimensional explicit finite difference program for engineering mechanics computation. This program simulates the behaviour of a structure built of soil, rock, or other materials that may undergo plastic flow when their yields limits are reached" ITASCA Consulting (Group 2011). The scenario to be tested is sectioned into zones which form a grid for the analysis. The user has the capability to set parameters for the shape of the soil body to be investigated. FLAC finds the static solutions for a problem using the two-dimensional plane-strain model. However, the dynamic equations of motion are included in the formulation to help model the stable and unstable forces within the model; this accounts for the sudden collapse within the model.

The basic explicit calculation cycle used in FLAC can be demonstrated in Figure 4; each complete cycle is considered one time step. The equations of motion are used to derive the velocities and displacements. New stresses and strain rates are calculated and the process continues until failure is achieved. Relatively small time step are chosen to ensure that the stress changes of each element do not influence its neighbours ITASCA Consulting (Group 2011).

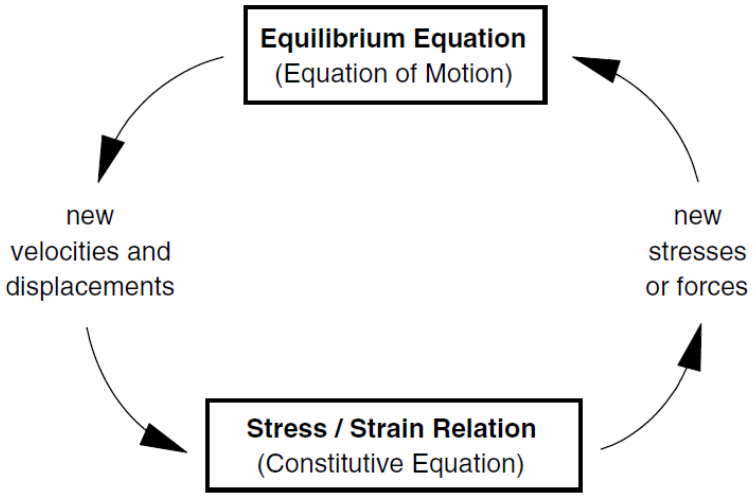

Figure 4 - Basic explicit calculation cycle (ITASCA Consulting Group 2011b)

The finite difference method is one of the oldest numerical techniques capable of the solution to sets of differential equations, with set boundary and/or initial values. With the finite difference method, every derivative component of the determining equations for the model is replaced with an algebraic expression which is written in the terms of the field variables; for example displacement or stresses at given points in the set up model space. FLAC uses explicit finite difference and regenerates each finite difference equation at each step. ITASCA Consulting (Group 2014).

The Finite difference method is based on the definition of the derivative of a function $f(x)$ (V.Hutton 2004):

$$\frac{d\,f(x)}{dx} = \frac{lim}{\Delta x \to 0}\left[\frac{(f(x+\Delta x) - f(x))}{\Delta x}\right]$$

The independent variable being x, in finite difference, small finite values of Δx are used to produce a solvable close approximation:

$$\frac{d\,f(x)}{dx} \approx \frac{f(x+\Delta x) - f(x)}{\Delta x}$$

This equation is then substituted into a differential equation to enable an approximate numerical solution. Hutton uses as an example the simple differential equation

$$\frac{d\,f}{dx} + x = 0$$

by expressing as

$$f(x+\Delta x) \approx f(x) - x\Delta x$$

(V.Hutton 2004) as well as the ITASCA Consulting group both demonstrate examples where the modelled solution is a close approximation to the exact solution. A limitation of the finite difference points calculated is that the difference

between these and the exact solution is not known (V.Hutton 2004), however decreasing the step size results in more iterations increases accuracy significantly.

FLAC uses the "Lagrangian" formulation since small displacements are added to the grid coordinates meaning the grid deforms with the material that it is modelling. At each step a small-strain is calculated, however, large-strains can be formed over may steps. ITASCA Consulting (Group 2014).

To model a situation in FLAC, a grid is set using quadrilaterals to connect four adjacent points. Each mesh quadrilateral is divided into two pairs of overlaid triangles representing constant strain triangular elements. (Figure 3.2) FLAC uses these pairs of Triangles to determine it the distortion is unacceptable.

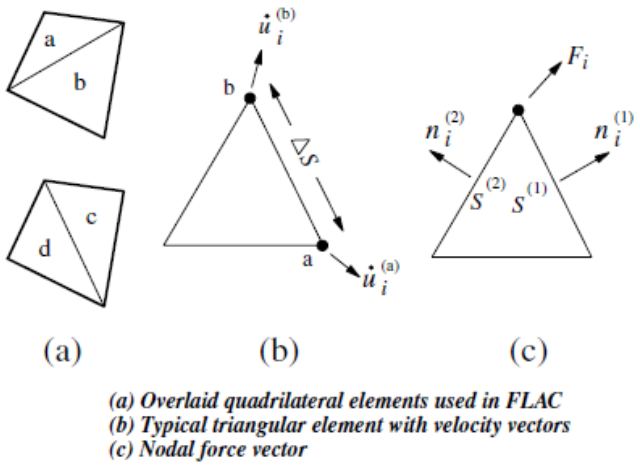

(a) Overlaid quadrilateral elements used in FLAC
(b) Typical triangular element with velocity vectors
(c) Nodal force vector

Figure 5 - Strain triangular elements (ITASCA Consulting Group)

Strain rates and strain for the overall zone are determined by using average velocity vectors obtained from triangular subzones. These values are determined using the following models.

$$\frac{\partial \dot{u}_i}{\partial x_j} \cong \frac{1}{2A} \sum_s \left(\dot{u}_i^{(a)} + \dot{u}_i^{(b)}\right) n_j \, \Delta s$$

$$\dot{e}_{ij} = \frac{1}{2}\left[\frac{\partial \dot{u}_i}{\partial x_j} + \frac{\partial \dot{u}_j}{\partial x_i}\right]$$

The maximum shear strain is the radius of the Mohr's circle as shown in Figure 6.

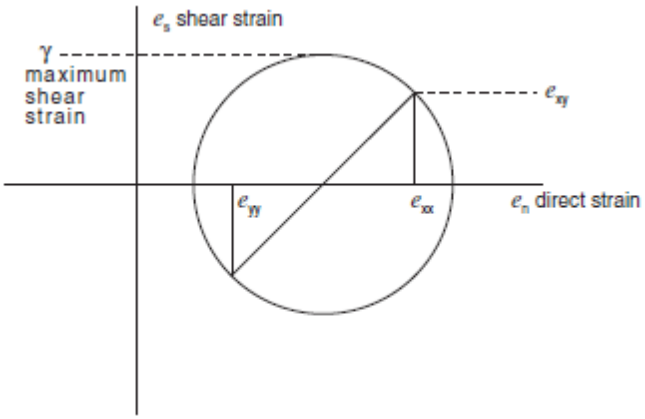

Figure 6 - Mohr's circle of strain

Therefore the two-dimensional plane-stress analysis, maximum shear strain γ is defines as:

$$\gamma = \frac{1}{2}\left((e_{xx} - e_{yy})^2 + 4e_{xy}^2\right)^{1/2}$$

This is the equation used to calculate the output in shear strain rate (ssr) plots. Explicit finite difference involves the reference to previously calculated point values which are progressively calculated at very small time steps to insure the accuracy of the model.

FLAC requires basic soil parameters to simulate the shear strength characteristic of a soil. In addition to the basic parameters, advanced properties may be provided as parameters where necessary.

3.2 Numerical Modelling Procedure in FLAC

The following are steps recommend to be taken to perform a successful numerical experiment in geomechanics, sourced from the Fast Lagrangian Analysis of Continua (FLAC) manual.

Step 1: Define the objectives for the model analysis

Understanding the main purpose of a geomechanic analysis allows for the required detail to be determined. This also will allow for minor complications that may have minimal effect on the final outcome to be neglected.

Step 2: Create a conceptual picture of the physical system

A conceptual picture helps clarify the probable or estimated outcomes of any modelling. It requires deeper thought into a number of questions regarding the imposed conditions or expected behaviour of the model. With the conceptual model, it is possible to decide on the best modelling structure and tools to implement for the numerical model.

Step 3: Construct and run simple idealised models

It is better to start any numerical analysis with a simple test model. Understanding of the idealised physical system may be formed and help with the development of more detailed models. It also allows for debugging of the numerical model if unexpected results are generated.

Step 4: Assemble problem-specific data

Numerical analysis is dependent on the parameters of the model to be conducted. These can be numerous depending on the geometry of the problem, material properties, initial conditions and at times external loadings. Many of these will have associated uncertainties and therefore a range of parameters needs to be selected for any investigation.

Step 5: Prepare a series of detailed model runs

In conducting numerical analysis using computer simulations a number of important aspects need to be taken into consideration to make the modelling via numerical analysis both efficient and effective. One consideration is the run processing time. If this is too long due to the complexity of the model, it may be beneficial to run a number of parameter variations on a number of computers to reduce the overall time for data collection.

Saving the model at a number of stages throughout the process can be time saving. Trials with changes to some parameters can be conducted without having to complete a full run if this practice is utilised correctly.

Having a number of checking locations in the model for comparing against physical data allows for clear interpretations to be made.

Step 6: Perform the model calculations

Initially is it best to conduct the first few detailed models individually and test to see if they are acting as expected. Once there is a high confidence level of the results, series of run can be conducted.

Step 7: Present results for interpretation

Presenting the data in both a manageable and easily understood format is imperative for clear analysis of the results. Results presented graphically using various plots allows for comparison with other investigations. Points of interest need be identified to assist in locating the major points of discussion.

ITASCA Consulting Manual - These steps assist in problem solving since they force the engineer to have a clear concept of what the model is intended to achieve.

Chapter 4

4.1 Analysis of Underground Trapdoors with zero Pressure Ratio

The strength reduction method for an underground trapdoor situation involving a zero pressure ratio has been investigated in this chapter. For simplicity and reduction of compute time, the underground trapdoor was simulated in a two dimensional context. FLAC software was used for this 2D analysis. With FLAC based upon the use of explicit finite differences, the soil mechanics of this situation has been modelled.

The two main purposes of this investigation are to determine the effect of the depth ratio and strength ratio on both the resulting factor of safety as well as to the extent of the surface failure of the underground sinkhole.

4.2 Problem definition and FLAC model

Figure 7 shows a problem schematic for the 2D model of a sinkhole. The height (*H)* represents the depth of overburden above the trapdoor; *W* represents the width of the trapdoor; σ_t is the supportive pressure and σ_s is the surcharge pressure. The undrained shear strength and the unit weight of the soil are represented by S_u and γ respectively.

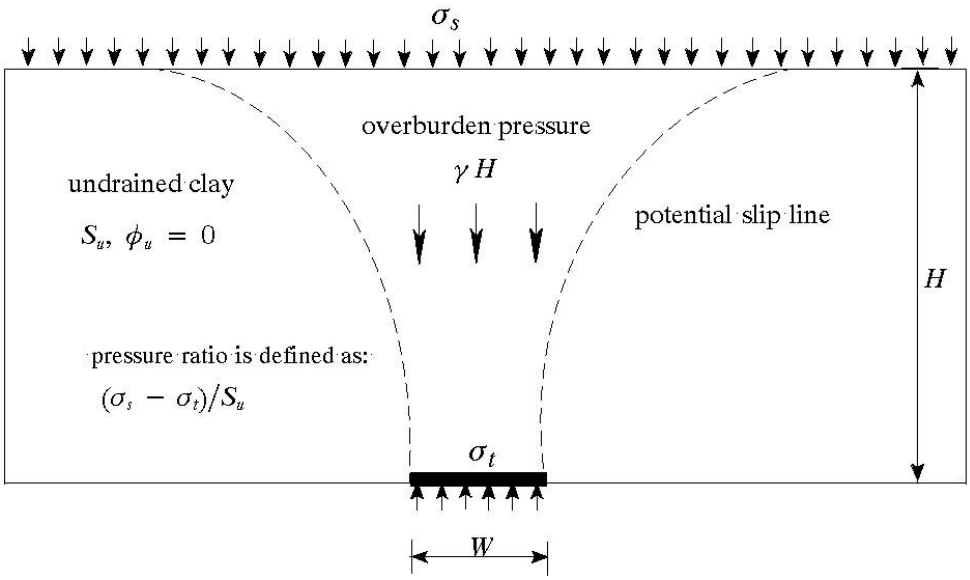

Figure 7 - Idealised sinkhole in 2D space

The two dimensional model has been constructed in FLAC using the material properties outlined above. Using Figure 7 it is possible to comprehend the three major dimensionless variables utilised in the FLAC model. The first variable is the ratio between the depths of the opening of the trapdoor to the width of the trapdoor. This is known as the Depth Ratio (H/W).

$$Depth\ Ratio = \frac{H}{W} \tag{4.1}$$

The second dimensionless variable is the Strength Ratio (SR), which is the ratio between the product of the unit weight of the soil and trapdoor width to the undrained shear strength of the soil. As an equation this is:

$$Strength\ Ratio\ (SR) = \frac{\gamma W}{S_u} \tag{4.2}$$

The third variable is the Pressure Ratio (N), which is the ratio between the change in surcharge pressure and internal pressure compared to the undrained shear strength.

$$Pressure\ Ratio\ (N) = \frac{\sigma_s - \sigma_t}{S_u} \tag{4.3}$$

In this chapter the pressure ratio is assumed to be zero as there are no external pressures applied to the model for initial testings.

Due to the use of the finite difference method, as explained in Chapter 3 it is necessary for boundary conditions to be set in both dimensions. This is an assumption for simplicity of modelling since the soil medium in which a sinkhole forms is a continuous entity where no specific fixed boundaries exist. Pretesting of the overall width of the boundaries was required to ensure no limiting effect was affecting the overall results.

The initial model had fixed boundary conditions for all points along the boundary, to be used as the reference condition. This was achieved by setting the horizontal boundary at the depth of the cavity opening to be fixed in both the horizontal and the vertical axis, whereas the vertical boundaries have been fixed only in the horizontal direction allowing for movement in the vertical plane. The boundary condition was then altered to simulate half the width of the required sinkhole at varying depths. To simulate the trapdoor scenario then required removing a section of the lower boundary to move freely in both dimensions. The FLAC model for a height to width ratio of 3 is shown in Figure 8.

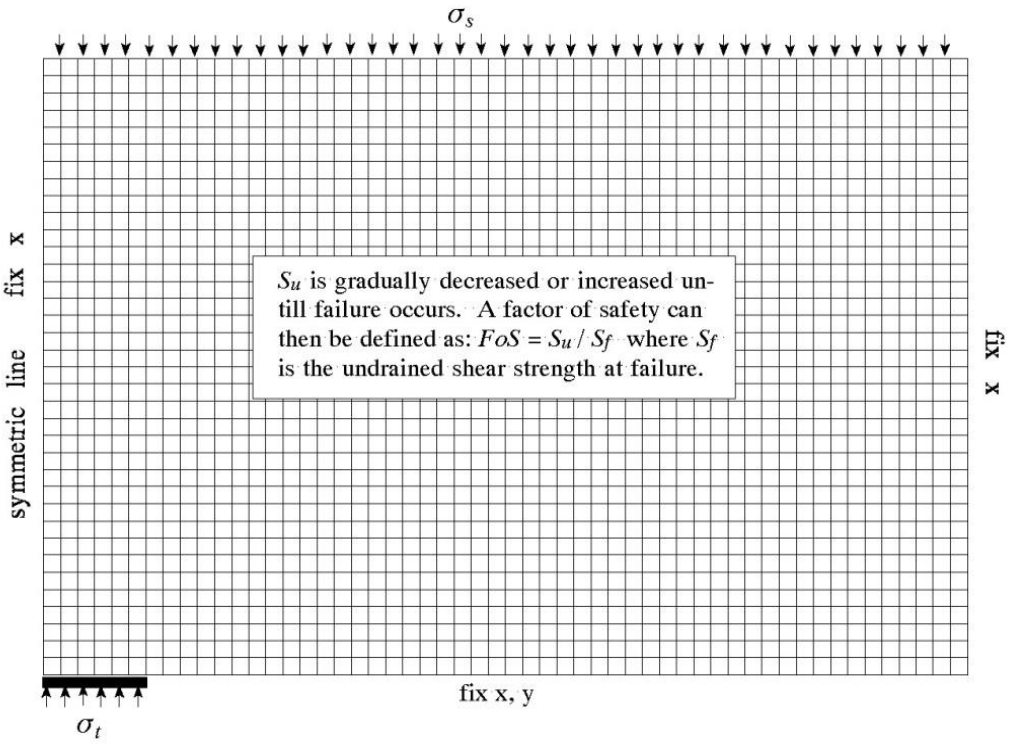

Figure 8 - Idealised sinkhole in 2D space (FLAC)

It is necessary to make these assumptions to enable the use of the FLAC software. Although this does not exactly simulate the real situation of the soil medium, it is necessary to make these assumptions in order to obtain useful results from the software package.

These models were then solved using the strength reduction method to calculate the factor of safety (FoS) as a measurement of the limiting strain versus the actual strain as discussed previously. A factor of safety of less than 1 indicates that the properties of the soil are inadequate to hold up the soil materials self-weight leading to failure.

The factor of safety (FoS) is dependent upon the depth ratio (H/W), the strength ratio (SR) and the pressure ratio (N). As stated above, in these initial tests the pressure ratio remains as a constant of zero and therefore the factor of safety can be expressed as a function of:

$$FOS = f\left(\frac{H}{W}, \frac{\gamma W}{S_u}\right) \quad (4.4)$$

To predict theoretical soil responses within cavity openings and overburden soil relationships, the use of simplification and assumptions in the model help to analyse the complexity of the physical soil conditions and overburden/ cavity interactions. The sinkhole model assumes the use of Mohr-Coulomb failure criteria with set soil characteristics of mass-density, elastic modulus, Poisson's ratio, cohesion and friction angle.

The material properties of the analysed undrained clay were assumed to have the following properties; Mass Density of 1834.86 kg/m^3, Elastic Modulus of 16 MPa, Poisson's ratio of 0.49, Tension of 10 GPa and no Friction Angle nor Dilation Angle. The tension ratio of 10 GPa is set this large to ensure that the failure of the model is due purely to shear failure and in tension. The chosen material was characteristically comprised of relatively high cohesion and zero friction angles allowing it to have stable unsupported capabilities.

This scenario was conducted multiple times with changes made to the cohesion of the over burdening soil. Elemental principal stresses, shear stain rates, velocity vectors, Y-displacements and plasticity indicators are to be plotted and discussed.

Within FLAC is a programming language known as FISH that gives the user the ability to define new variables and functions. These functions may be utilised to enhance the usefulness of FLAC through the application of these user defined features.

Sometimes FLAC's built-in grid generators will not be able to produce a desired geometry. A series of INITIAL commands can always be used to specify locations of individual grid points if all else fail. This can be tedious if every x- and y-point must be specified individually, but it is often possible to write a program that generates the grid automatically using the built-in programming language, FISH. (ITASCA Consulting Group 2014)

Within this investigation the FISH programming language is utilised to generate the required grid to simulate the geometry and geology of the region surrounding the trapdoor collapse. The FISH script was designed as part of this investigation by the

Tunnelling Research Group, of which this thesis is a product. The script sets the soil properties, mesh size and geometry of half a trapdoor scenario.

4.3 Comparison of Results

Factors of Safety have been obtained for unsupported trapdoors in cohesive soil using the strength reduction method and FLAC finite difference method. The analysis of the data uses two parameters, including the depth ratio (H/W) and strength ratios (γW/Su).

The raw data obtained from the shear strength reduction method (SSRD) is recorded in Appendix C. This data has been summarised for comparison against previous studies carried out by Davis (1968), Gunn (1980) and Sloan (1990) in Table 1.

Table 1 – Comparison to Previous works

	Davis (1968)		Gunn (1980)		Sloan et al. (1990)		This Study
H/W	L.B.	U.B.	L.B.	U.B.	L.B.	U.B.	F.D
1.0	1.60	2.00	1.40	1.85	1.75	2.00	2.16
2.0	3.40	3.95	2.70	-	3.60	3.90	3.89
3.0	3.70	6.00	3.60	4.90	4.50	5.00	4.93
4.0	3.90	7.90	4.20	5.80	5.20	5.80	5.64
5.0	3.95	10.00	4.50	6.40	5.45	6.20	6.20
6.0	3.95	-	4.90	7.10	6.10	6.75	6.66

The factor of safety, found in this study when the H/W ratio was equal to 1, lay outside the upper bound of the three previous studies used for comparison.

As the depth to width ratio increased, the values obtained compared favourably for all other ratios indicating that the finite difference and strength reduction method is a viable alternative when analysing the stability of trapdoors.

The finite difference results indicate a strong correlation with the upper bound solutions of the three previous studies. Graphically this comparison is shown in figure 4.3. It suggests that the techniques used in this study lie within the upper and lower bounds of the three previous studies over the past 50 years.

Generally the data correlates more closely to the upper bounds of Gunn (1980) and Sloan (1990). The modelling approach undertaken in this investigation using the strength reduction method through the use of the FLAC software can therefore be assumed to be viable.

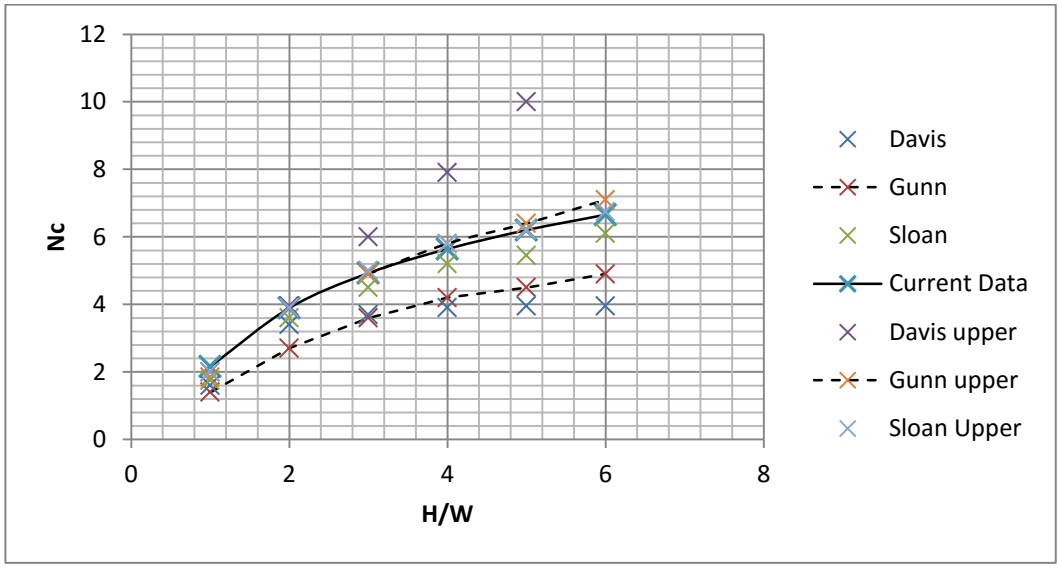

Figure 9 – Graphical Comparison with Previous Studies

4.4 Results Discussion

4.4.1 Results for Stability Number (N) = 0

Factors of safety have been obtained for unsupported trapdoors in cohesive soil using the strength reduction method and FLAC finite difference method. The analysis of the data uses two parameters, including the depth ratio (H/W) and strength ratio (γW /Su). The factor of safety (FoS) has been plotted against both the strength ratio and height to width ratio shown in figure 10 and figure 11 respectively.

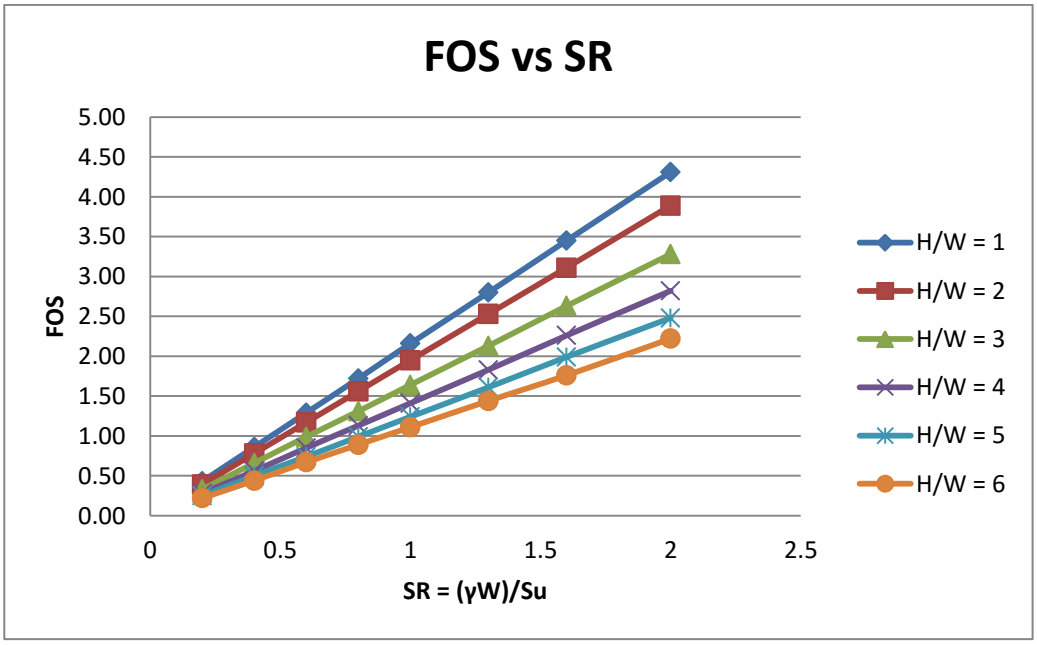

Figure 10 – Factor of Safety vs the Strength Ratio

Graphically, the results of the study for factor of safety against strength ratio *γW*/Su are shown in Figure 10. It appears that the FOS of the Trapdoor is directly proportional to the strength ratio ($\gamma W/S_u$). The constant of proportionality decreases as the depth to width ratio (H/W) increases indicating that deeper trapdoors have greater benefit from increasing soil shear strengths compared to shallow trapdoors.

Analysing the same data by comparing the factor of safety to the ratio of height to width, indicates a rough inverse relationship between the two variables as seen in

Figure 11. This again indicates that the factor of safety increases as the strength ratio rises and decreases as the height to width ratio increases.

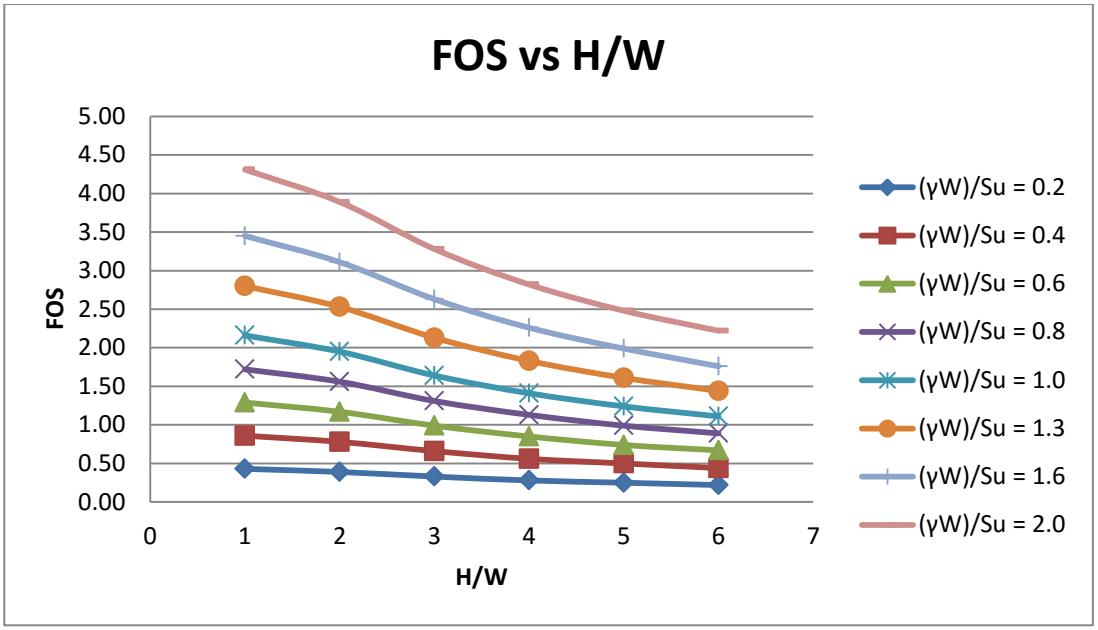

Figure 11 – Factor of Safety vs Height to Width Ratio

4.4.2 FLAC Outputs for Stability Number (N) = 0

The shear strain rate can be defined as the rate of change in strain or deformation of the soil body with respect to time. Due to the assumption that there is no surcharge or internal pressure about the trapdoor, gravity is the only force acting on the soil body. This creates a parallel stress of shearing slippage. Figure 12 is an example of the shear strain output obtained from FLAC. The maximum shear strain rate can be seen to be occurring around the cavity opening and as the deformation is the main feature being measured in this plot, the slip planes can be easily identified by the parallel contours. A chimney type failure is exhibited which is identified by the curved slip plane.

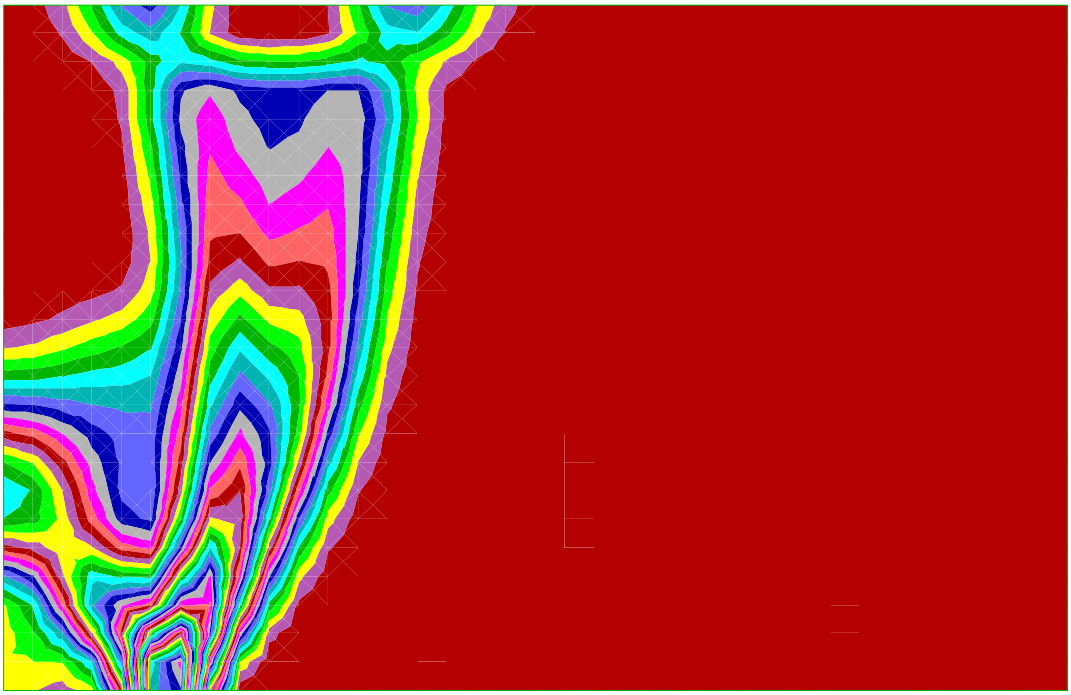

Figure 12 – Shear Strain Rate (SSR) Plot (H/W=2 SR=0.8)

Figure 13 allows for comparison of soils of different strengths ratios while keeping a depth ratio of 2 which is a relatively shallow case. The strengths ratios vary from 0.2 up to 2. The eight cases compared in this figure visually indicate that changing the strength ratio has minimal effect to the overall appearance of the slip plane. It also is noticed that even though the strength ratio has increased by an overall factor of ten, the change in the extent of surface failure is minimal. This suggests that the strength ratio does not have a major impact on the resulting sinkhole formed under these conditions.

When observing the raw data, it can be seen that the variations of the strength ratio does have a noticeable effect on the stability of the trapdoor. The numerical data indicates that for smaller strength ratios, the scenario is unstable due to an achieved factor of safety of less than 1. As the strength ratio increases the resulting factor of safety increases, indicating a more stable scenario.

Figure 14 shows similar plots for a depth ratio of 5, the obvious difference is the number and size of the contours around the cavity opening which is true for each strength ratio. This indicates the increased pressure above the cavity due to the

increased weight of the soil due to its depth. The decrease in maximum factor of safety indicates that with deeper cases, collapse is more eminent.

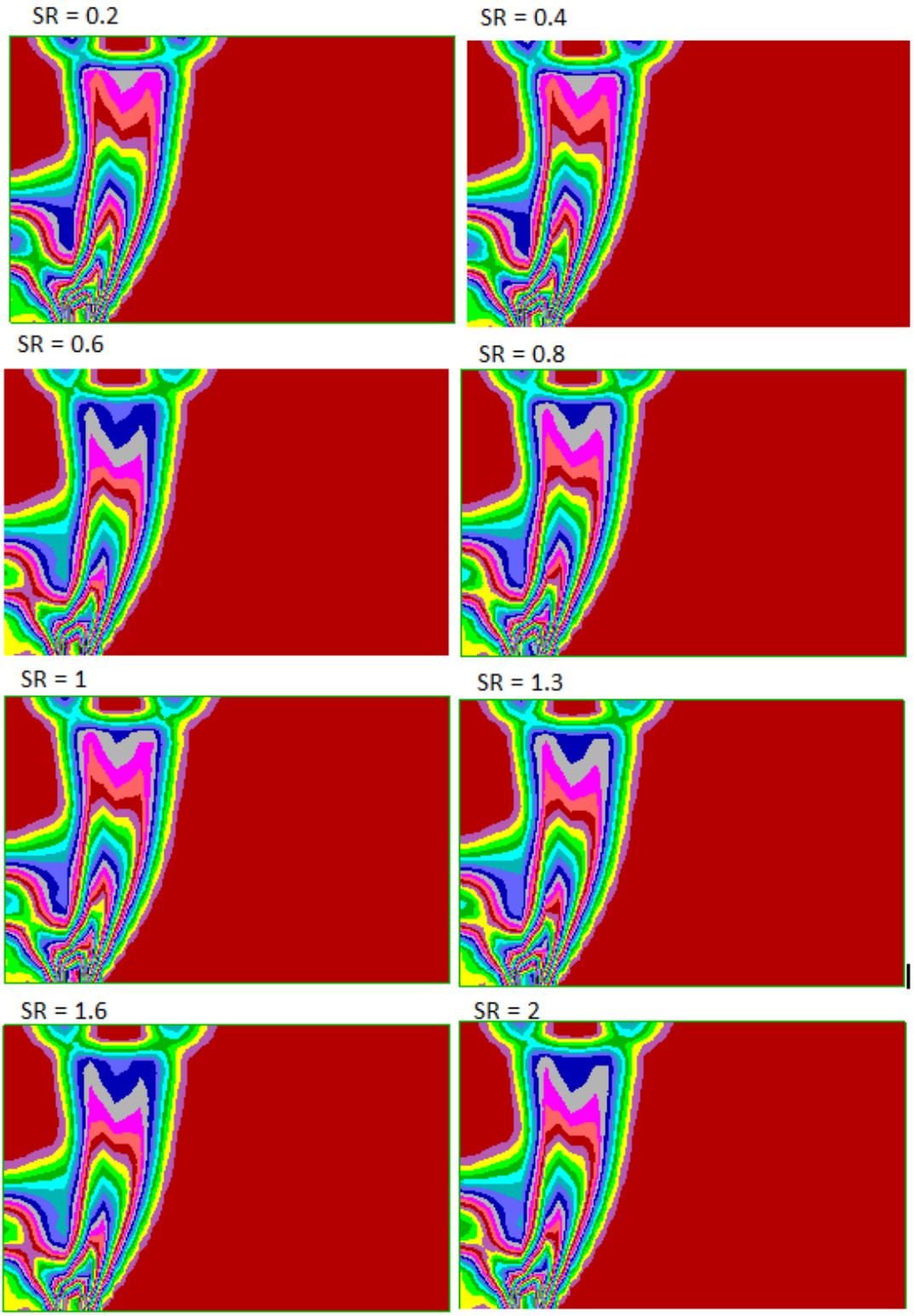

Figure 13 – Shear Strain Rate (SSR) Plots (H/W=2)

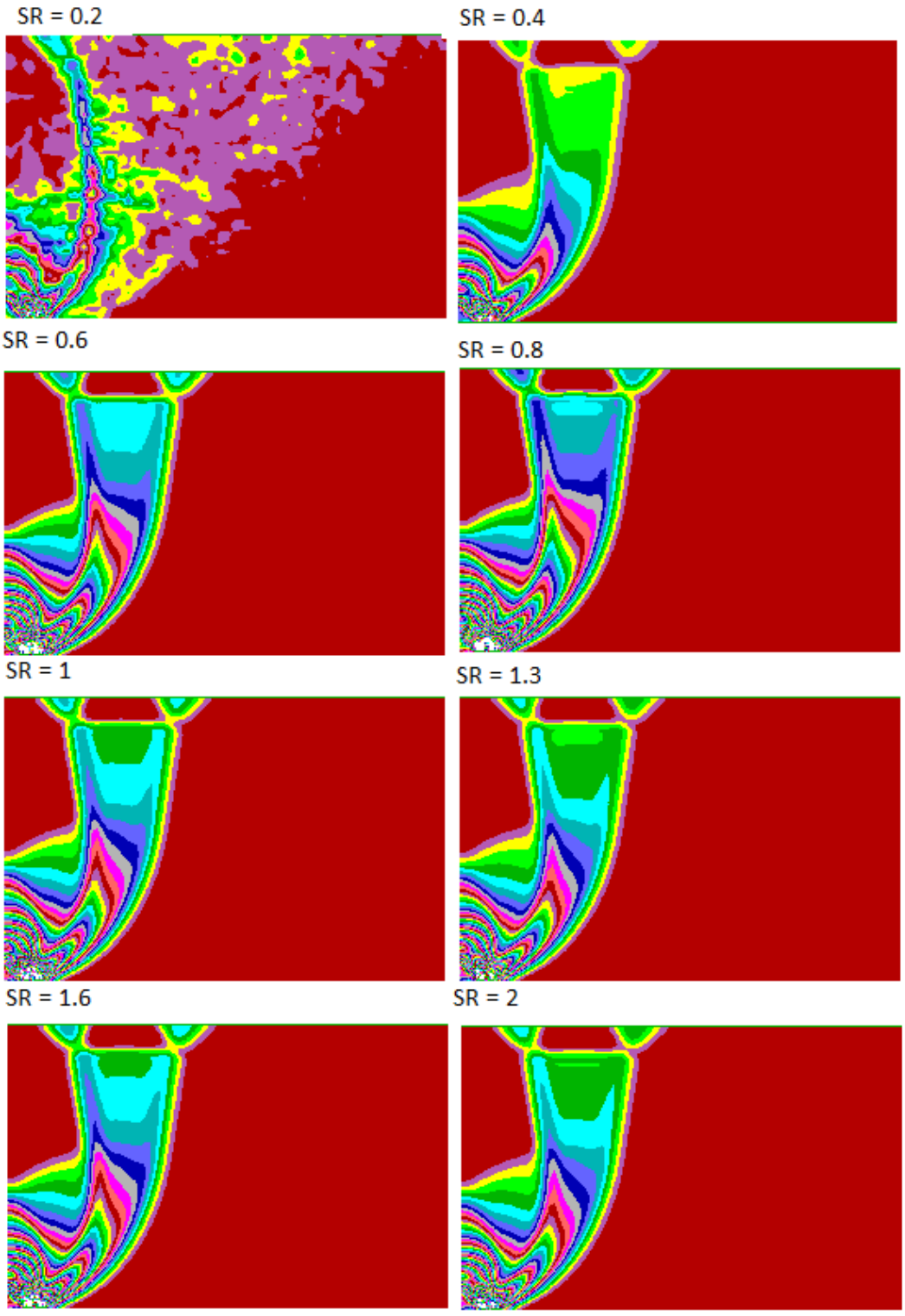

Figure 14 – Shear Strain Rate (SSR) Plots (H/W=5)

To obtain a visual impact of the effect of the change in depth to width ratio, the strength ratio was fixed at SR = 1 and the six shear strain rates where plotted in figure 15. There are obvious differences in both shape and the number of shear strain rate contours as the depth to with ratio increases.

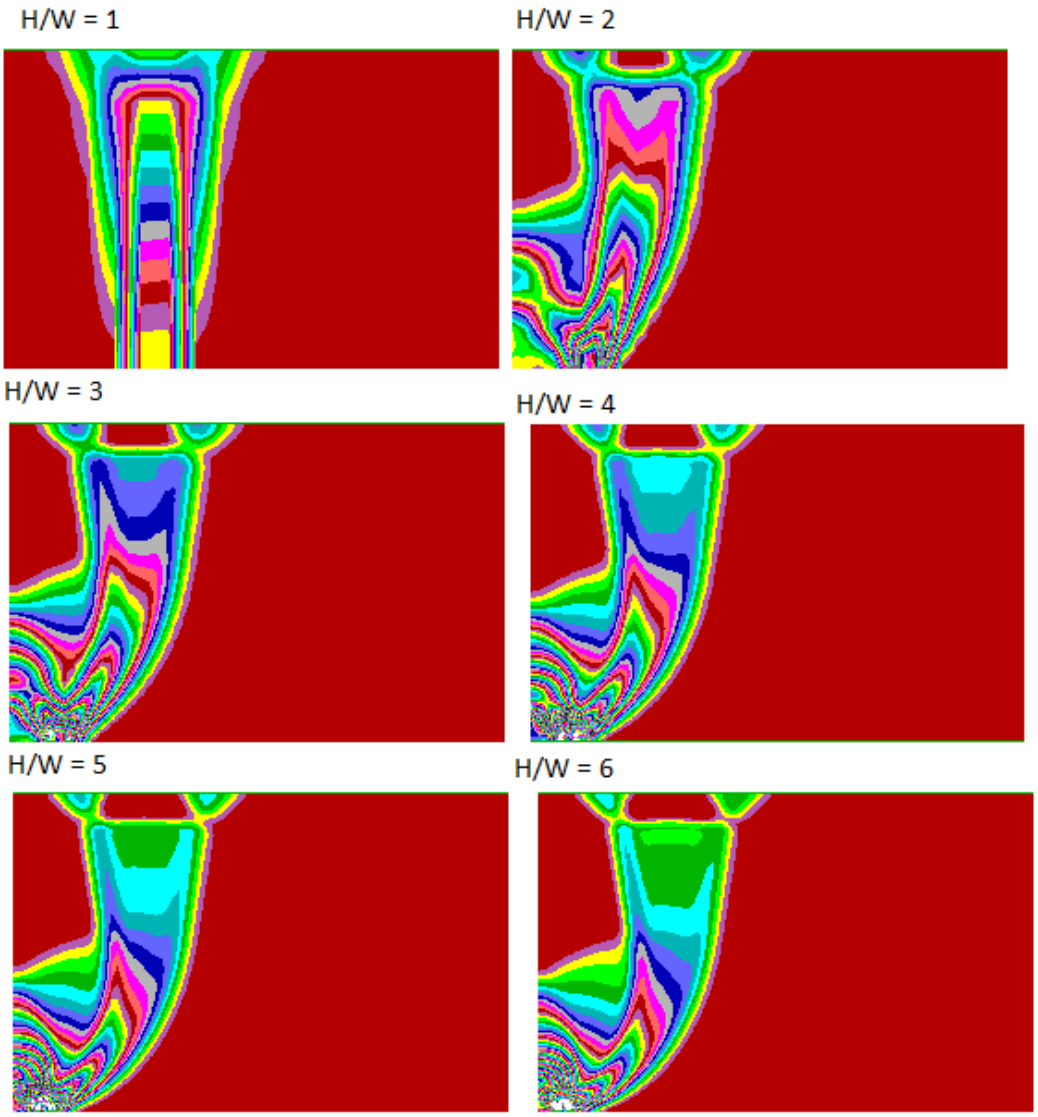

Figure 15 – Shear Strain Rate (SSR) Plots (SR=1)

The first impact is the extent of the surface failure as the depth ratio increases. With a depth ratio of one, the model for half the sink hole was 3 metres at the trapdoor. The resulting width of the surface failure was 4.8 metres. When the depth ratio was increased to 6 the extent of the surface failure increased to a width of 25.5 metres.

This indicates that the deeper the trapdoor failure the greater the extent of the surface failure. The strain within the overburden is reduced due to the central failure at the trapdoor and hence greater lateral collapse into the sinkhole.

Table 2 – Surface Failure Ratios

Depth Ratio	Extent of Surface failure (m)	Surface failure/Cavity Width
1	4.8	1.60
2	8.6	2.87
3	12.8	4.27
4	17.1	5.70
5	21.3	7.10
6	25.5	8.50

The extent of the surface failure compared to the depth ratio has been recorded in Table 2 above. As the depth ratio increased, from the smallest ratio to the largest ratio, by a factor of six the surface failure increased from a measurement of 4.8 metres to a measurement of 25.5 metres. The extent of the surface failure has increased by a factor less than 6; however, there is a strong relationship between the surface failure ratio and the depth ratio. This has been graphed in figure 16. The greater surface failure compared to the trapdoor width is justification of the conical shape of sinkhole collapse.

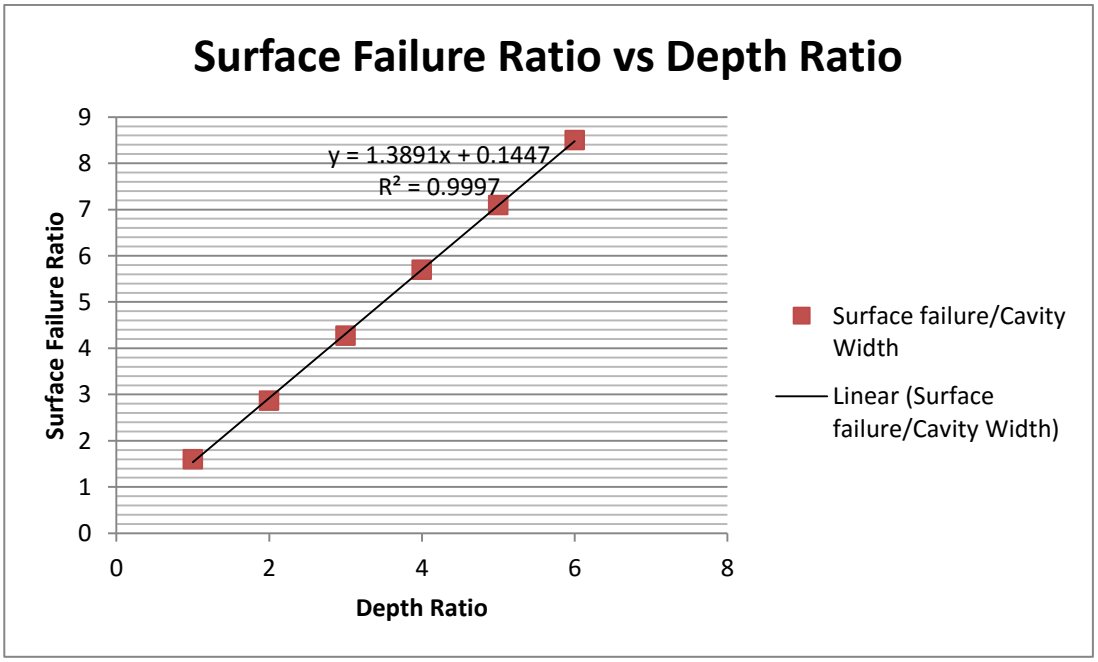

Figure 16 – Surface Failure Ratio Plot

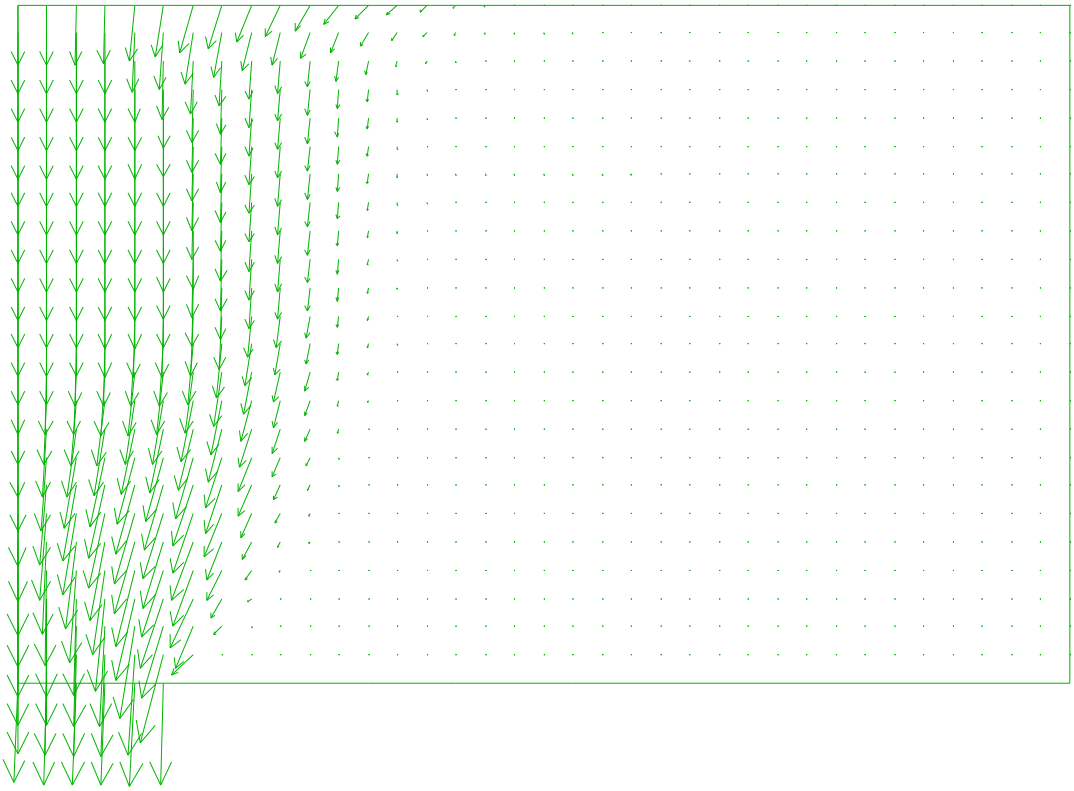

Figure 17 – Velocity Vector Plot (H/W=2 SR=0.8)

Velocity vectors represent the rate of change of position of the soil particles, with the magnitude of the vector indicating speed and the bearing giving direction. Overall this illustrates the movement of the collapsing soil over a period of time. An example of velocity vectors with a depth ratio of H/W = 2 and a strength ratio of SR = 0.8 is shown in figure 17. The shorter vectors along the slip surface indicate slower movement of soil due to friction and the direction of these vectors is tangential to the slip surface; whereas in the centre of mass of the sinkhole the motion is purely vertical, having a greater velocity. All of the effected overburdening soil is being funneled towards the opening of the cavity; this is seen by the density of the vectors.

The force that maintains the rigidity of a group of particles is known as the 'effective principle stresses'. These stresses can be easily disturbed by the application of additional forces on the soil body. When analysing figure 17, it can be observed that the stresses are being shifted from the yielding parts of the soil

mass to the adjacent non yielding parts. This movement is opposed by a shearing resistance that occurs inside the zone of contact of the adjacent masses. This notable transfer of pressure between masses of soil is commonly known as the arching effect, and the soil is said to arch over the yielding part of the support.

Compressive stresses caused by the self-weight of the overburdening soil and gravity are relocated by the arching effect. This is an attempt by the soil to self-support its own weight to prevent the event of a collapse. The arching effect seems to relocate the stresses in such a way that it appears that there is no compressive stresses acting directly above the cavity opening.

Figure 18 to Figure 20 demonstrate the change in arching effect as the depth ratio increases from 2 through 4 to 6. The effect is noticed at each depth, however, the arching effect has a greater magnitude the shallower the underground trapdoor.

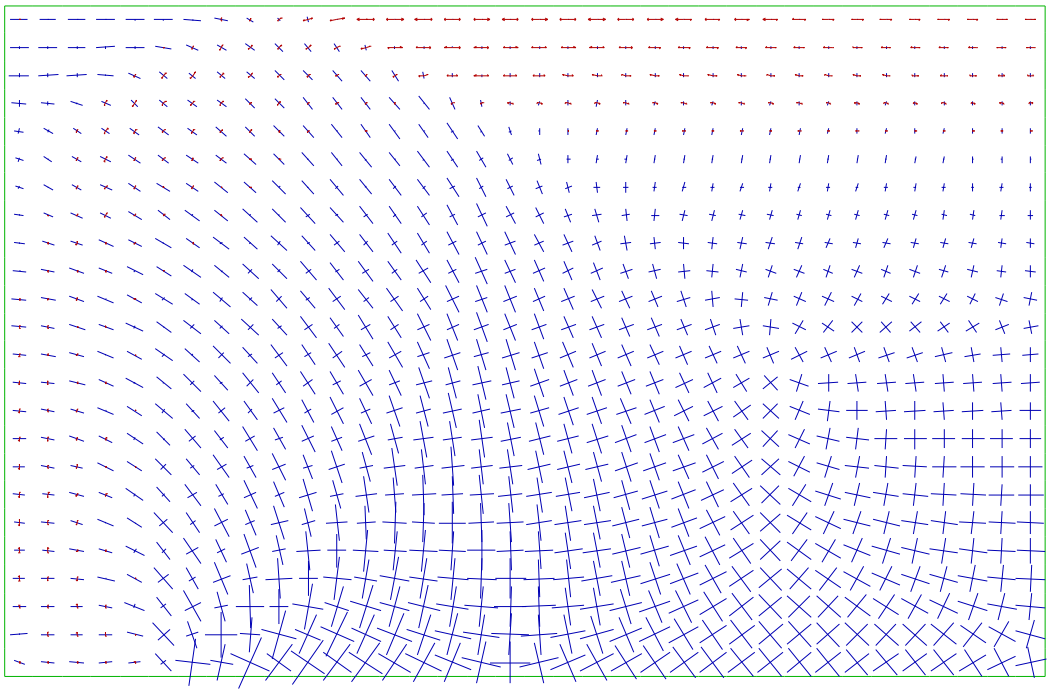

Figure 18 Plot of Effective Principle Stresses for H/W=2 and γW/Su =0.8

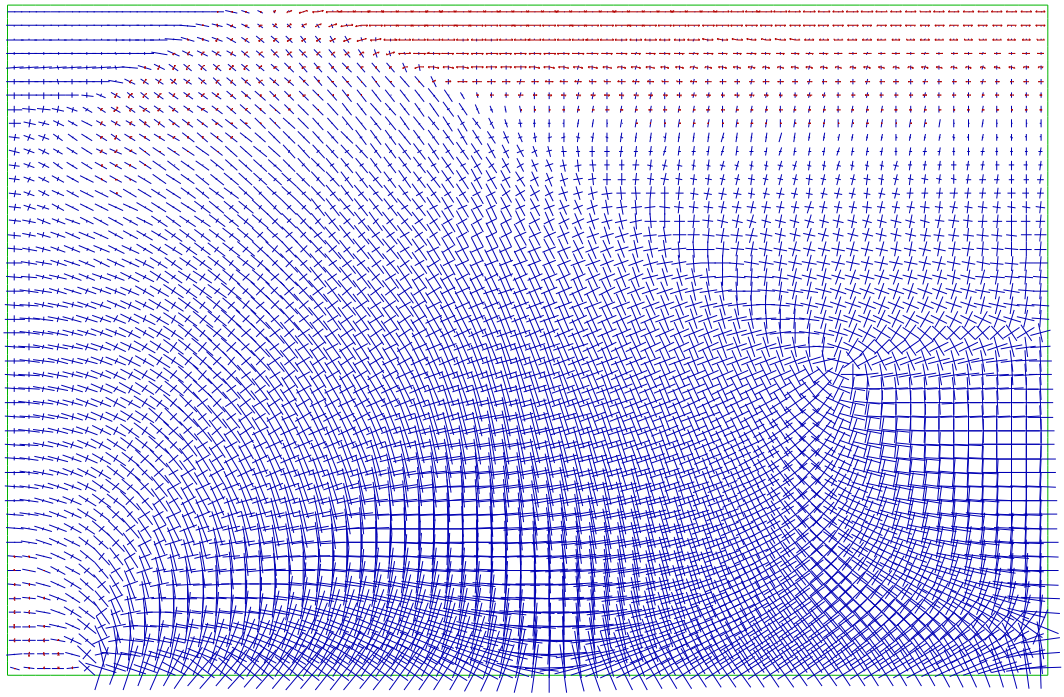

Figure 19 – Plot of Effective Principle Stresses for H/W=4 and γW/Su =0.8

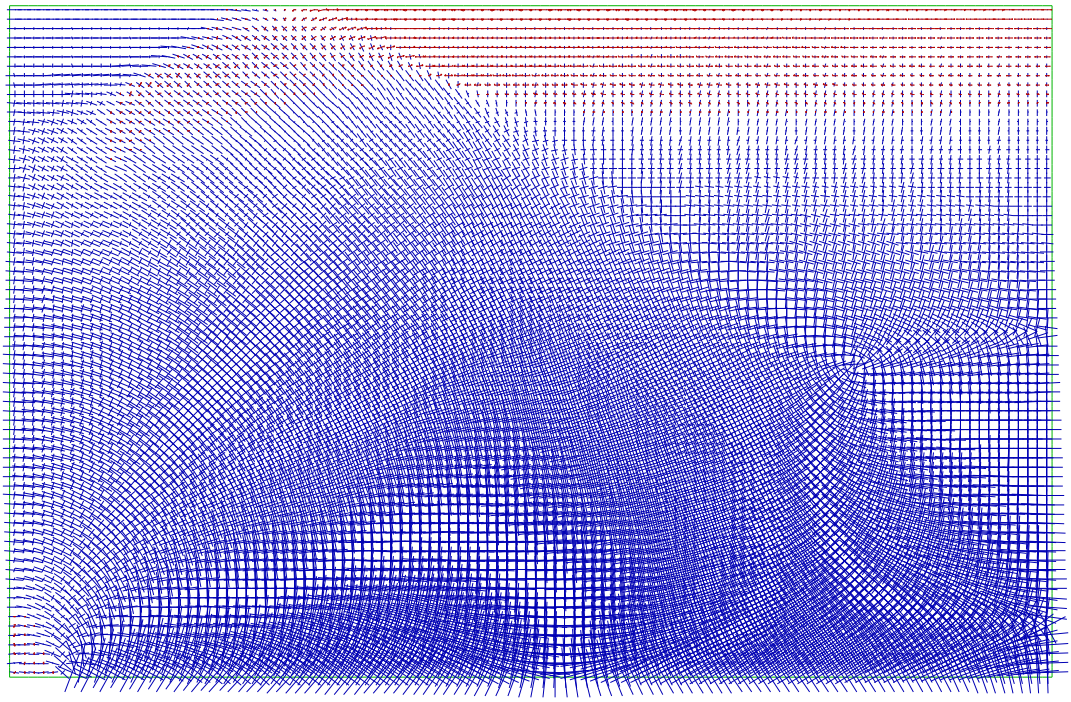

Figure 20 – Plot of Effective Principle Stresses for H/W=6 and γW/Su =0.8

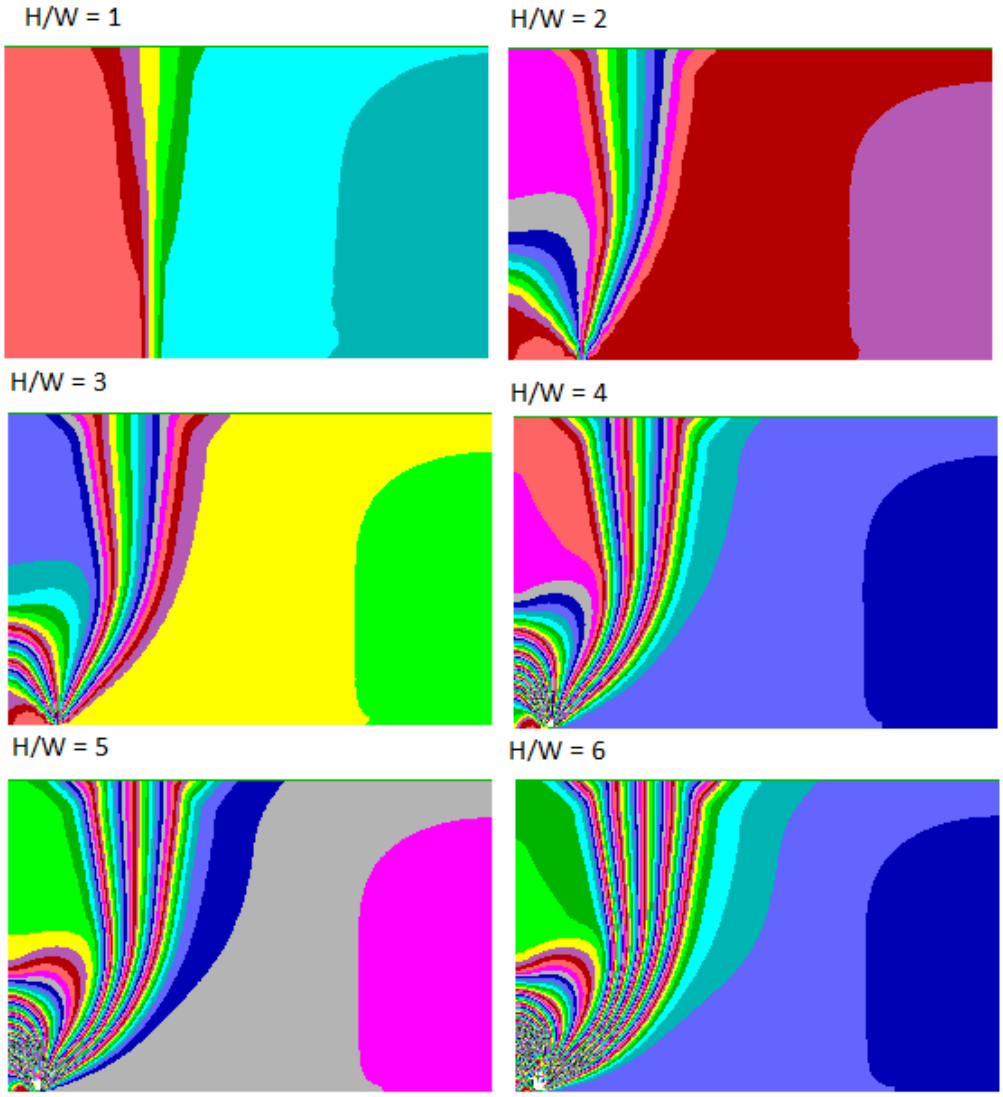

Figure 21 – Y Displacement Contours (SR=1) Comparison

Figure 21 shows the y-displacement contour plots with strength ratios of 1 at varying depth ratios. It is clear that the number of contours increases as the depth ratio increases. This is predicted as the deeper the cavity the smaller the displacement of contour widths. It can be seen that the realignment of the stresses is more apparent in the deeper cases to support the greater overburdening self-weight, hence the wider impact on the surface.

Using FLAC it is also possible to produce plasticity indicator plots. Figure 22 plots the indicators for the scenario of a depth ratio of 2 with a strength ratio of 0.8. The red indicators are points that are presently yielding where there is possible plastic failure. The green indicators represent past yielding, and where there has been no indicator produced signals points that represent no yielding or elastic behaviour in the soil.

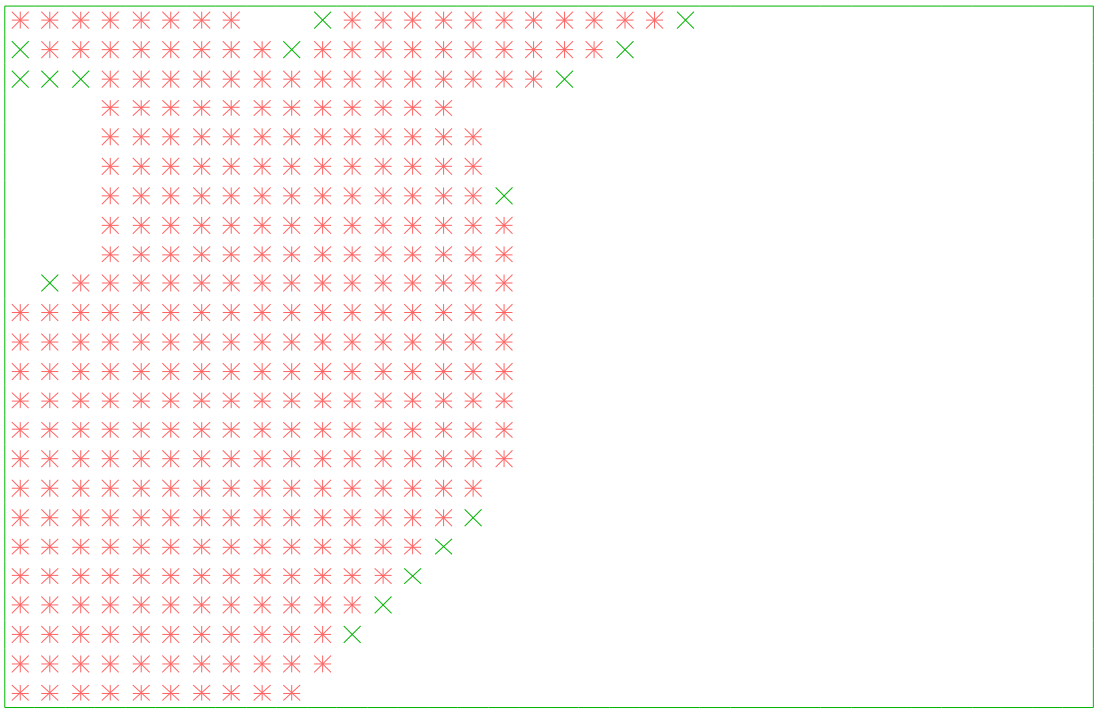

Figure 22 – Plasticity Indicator plot (H/W=2 SR=0.8)

The plasticity indicators have also been plotted over the shear strain rate contour plot as seen in Figure 23. The red plasticity indicators confirm that yielding and plastic deformation has occurred throughout the overburden. This gives a clear indication of the sinkhole collapse mechanics for this case, as both plots complement each other. Having these plots coincide increases the confidence level with regards to finding possible slip planes within the overburden above the underground cavity.

Figure 23 – Plasticity Indicator plot and SSR plot Comparison

4.5 Stability Chart and Practical Uses

Using the raw data obtained from analysis and shown in tables 1 and 2, a design contour chart has been constructed and shown in figure 24. This chart relates the depth to width ratio, soil strength ratio and the factor of safety by plotting these relevant parameters clearly on the one chart. This makes it a simple and useful approach that can be used by engineers for analysis purposes.

Figure 10 indicates that the factor of safety for any given height to width ratio was directly proportional to the strength ratio. Figure 11 suggests that the factor of safety also has an inverse relationship to the height to width ratio. Regression techniques indicate that the relationship between these three variables can be modelled in the form of:

$$FOS = f\left(\frac{H}{W}, \frac{\gamma W}{S_u}\right) \quad (4.5)$$

After executing the previously stated methodology over a large number of trials, a possible relationship relating these variables is:

$$FoS = \left(\frac{\gamma W}{S_u}\right)\left(\frac{1}{0.14\left(\frac{H}{W}\right)+0.15}\right) \qquad (4.6)$$

This model has a correlation coefficient of 0.98, which would suggest a strong model. This model behaves as expected since the more cohesive the soil the greater the factor of safety. Also since the width of the modelled trapdoor was fixed, by changing the height this increases the depth to width ratio which in turn decreases the factor of safety. This again validates that the deeper the trapdoor with respect to the trapdoor width, the overburdening soil is less stable due to its self-weight.

The raw data has been graphically represented in figure 24. A similar chart would be obtained if the derived equation had been used. This chart can be used in a practical context to simplify the determination of the factor of safety for any given scenario in homogeneous undrained clay given the strength ratio height to width ratio.

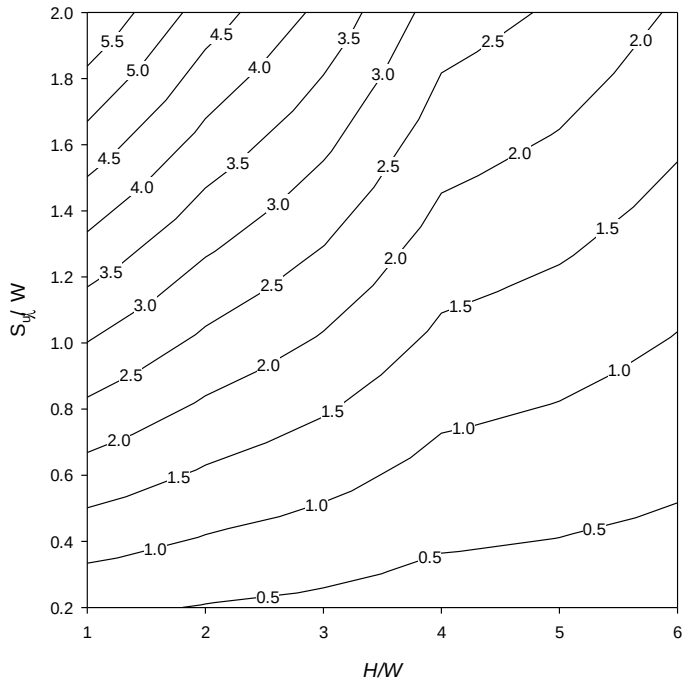

Figure 24 - Stability chart for FoS with respect to H/W and Su/γW

For example:

Given the parameters of undrained shear strength, density and depth and width of trapdoor stated below, it is possible to efficiently estimate the factor of safety.

$\mathrm{Su} = 30\mathrm{kPa}, \gamma = 18\ \mathrm{kN}/m^3, H = 6\ m, W = 2\ m$

This results in a depth ratio (H/W) of 3, and a strength ratio (γW/Su) of 0.83.
Using equation 4.2 with these parameters predicts an FOS of 1.46.
Using the same parameters with Figure 24 results in an FOS slightly greater than 1.50

As can be seen from the two results, the loss in precision can be accounted for by the simplicity of determining an accurate factor of safety graphically.

Alternatively, the chart can be worked in the opposite direction. If given the properties of FoS, undrained shear strength and soil density the required depth ratio (H/W) can be resolved.

$\mathrm{FoS} = 2, \mathrm{Su} = 30\mathrm{kPa}, \gamma = 18\ \mathrm{kN}/m^3$

This results in a Strength Ratio (γW/Su) of 0.83

Rearranging equation 4.6 to make H/W the subject:

$$FoS = \left(\frac{\gamma W}{S_u}\right)\left(\frac{1}{0.14\left(\frac{H}{W}\right) + 0.15}\right)$$

$$\frac{FoS}{\left(\frac{\gamma W}{S_u}\right)} = \left(\frac{1}{0.14\left(\frac{H}{W}\right) + 0.15}\right)$$

$$\frac{\left(\frac{\gamma W}{S_u}\right)}{FoS} = 0.14\left(\frac{H}{W}\right) + 0.15$$

$$\left(\frac{H}{W}\right) = \frac{\left(\frac{\gamma W}{S_u}\right)}{\frac{FoS}{0.14}} - 0.15$$

$$\left(\frac{H}{W}\right) = 1.90$$

Using the same parameters with Figure 24, results in a depth ratio of roughly 2. As can be seen from the two results, the loss in precision can be accounted for by interpolation in determining an accurate depth ratio graphically.

These two examples show how this stability chart can be used in practice when applying different scenarios restrictions to achieve the missing piece of data required by the user.

Chapter 5

5.1 Analysis of Underground Trapdoors with Non-Zero Pressure Ratio

In the previous chapter, the simplified model was explored where there were no external forces applied to the overburdening soil body. In this chapter the introduction of these external forces will be analysed in varying configurations. Briefly, the external forces being applied can be broken up into two categories, one being the surcharge which is a positive force acting in the same direction as gravity (σ_s) and the other being the internal pressure within the cavity which is considered a negative force acting in the opposite direction (σ_t). The positive forces are applied on the surface level of the overburdening soil and add additional weight that the trapdoor must support. These forces can range from manmade structures in the form of buildings or natural weights such as bodies of water or snowfall. The second group of forces act upward pushing against the bottom of the trapdoor which aid in the support of the overburdening soil. These forces can be in the form of air pockets or large bodies of moving underground water.

5.2 Problem definition and FLAC model

Figure 25 shows the problem schematic for the 2D model of a sinkhole. The height (*H)* represents the depth of overburden above the trapdoor; *W* represents the width of the trapdoor; σ_t is the supportive internal pressure and σ_s is the surcharge pressure. The undrained shear strength and the unit weight of the soil are represented by S_u and γ respectively.

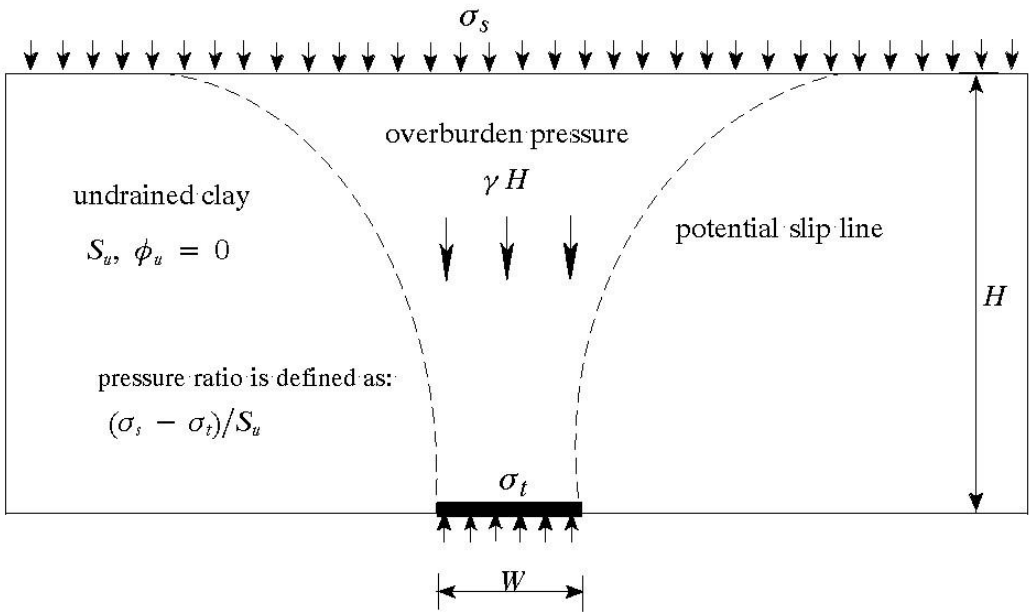

Figure 25 - Idealised sinkhole in 2D space

The two dimensional model has been constructed in FLAC using the material properties outlined above. Using Figure 25 it is possible to comprehend the three major dimensionless variables utilised in the FLAC model. The first variable is the ratio between the depths of the opening of the trapdoor to the width of the trapdoor. This is known as the Depth Ratio (H/W).

$$Depth\ Ratio = \frac{H}{W} \tag{5.1}$$

The second dimensionless variable is the Strength Ratio (SR), which is the ratio between the product of the unit weight of the soil and trapdoor width to the undrained shear strength of the soil. As an equation this is:

$$Strength\ Ratio\ (SR) = \frac{\gamma W}{S_u} \tag{5.2}$$

The third variable is the Pressure Ratio (N), which is the ratio between the change in surcharge pressure and internal pressure compared to the undrained shear strength.

$$Pressure\ Ratio\ (N) = \frac{\sigma_s - \sigma_t}{S_u} \tag{5.3}$$

In this chapter the pressure ratio is assumed to be non-zero as there are now external pressures applied to the model for initial testings. The combination of these forces ($\sigma_s - \sigma_t$), when compared to the undrained shear strength of the soil (S_u), provides the now valid pressure ratio.

Now that the pressure ratio comes into play when analysing the model, it is possible for the failure to be either a collapse failure or a blowout failure. This means that the model now depends on the variables mentioned above.

Due to the inclusion of the pressure ratio, the factor of safety now becomes a function of the depth ratio, strength ratio and the pressure ratio.

$$FOS = f\left(\frac{H}{W}, \frac{\gamma W}{S_u}, \frac{\sigma_s - \sigma_t}{S_u}\right) \quad (5.4)$$

To enable a direct comparison to the results from Wilson et al. (2011) this model can be modified to use the critical strength and pressure ratios. These can be conveniently converted from both the strength and pressure ratios by multiplying both by the factor of safety. These are the dimensionless strength and pressure ratios which maintain stability (FoS = 1). They will be used as a check of the model formed in this investigation.

The Critical Pressure Ratio and Critical Strength Ratio are calculated using:

$$Critical\ Pressure\ Ratio\ (N_c) = \frac{\sigma_s - \sigma_t}{S_u}.FoS \quad (5.5)$$

$$Critical\ Strenght\ Ratio\ (SR)_c = \frac{\gamma W}{S_u}.FoS \quad (5.6)$$

Using these critical ratios, the factor of safety now becomes a function of the depth ratio, critical strength ratio and the critical pressure ratio.

$$N_c = f\left(\frac{H}{W}, \frac{\gamma W}{S_u}\ FoS\right) \quad (5.7)$$

As previously stated, due to the use of the finite difference method, as explained in Chapter 3, it is necessary for boundary conditions to be set in both dimensions. This is an assumption for simplicity of modelling since the soil medium in which a sinkhole forms is a continuous entity where no specific fixed boundaries exist. Pretesting of the overall width of the boundaries was required to ensure no limiting effect was altering the overall results.

The initial model had fixed boundary conditions for all points along the boundary, to be used as the reference condition. This was achieved by setting the horizontal boundary at the depth of the cavity opening to be fixed in both the horizontal and the vertical axis, whereas the vertical boundaries have been fixed only in the horizontal direction allowing for movement in the vertical plane. The boundary condition was then altered to simulate half the width of the required sinkhole at varying depths. To simulate the trapdoor scenario, it is necessary to remove a section of the lower boundary for the soil to move freely in both dimensions. The FLAC model for a height to with ratio of three is shown in Figure 26.

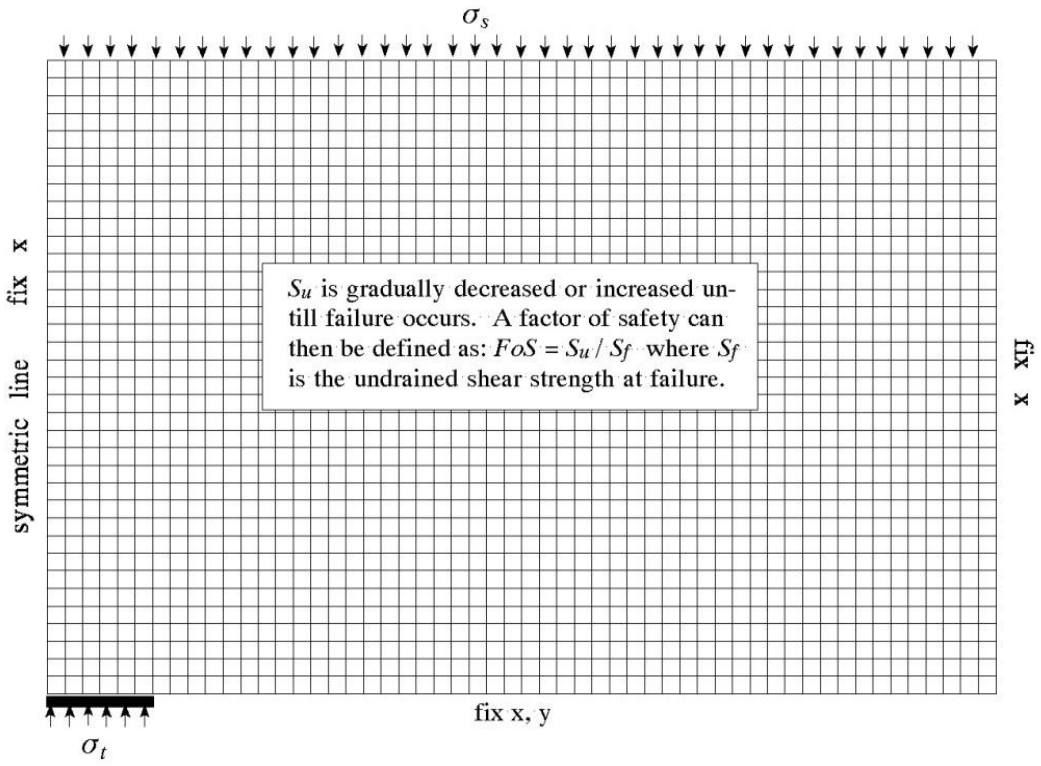

Figure 26 - Idealised sinkhole in 2D space (FLAC

It is necessary to make these assumptions to enable the use of the FLAC software. Although this does not exactly simulate the real situation of the soil medium, it is necessary to make these assumptions in order to obtain useful results from the software package.

These models were then solved using the strength reduction method to calculate the factor of safety (FoS) as a measurement of the limiting strain versus the actual strain as discussed previously. A factor of safety of less than 1 indicates that the properties of the soil are inadequate to hold up the soil materials self-weight leading to failure.

To predict theoretical soil responses within cavity openings and overburden soil relationships, the use of simplification and assumptions in the model help to analyse the complexity of the physical soil conditions and overburden/ cavity interactions. The sinkhole model assumes the use of Mohr-Coulomb failure criteria with set soil characteristics of mass-density, elastic modulus, Poisson's ratio, cohesion and friction angle.

The material properties of the analysed undrained clay were assumed to have the following properties; Mass Density of 1834.86 kg/m^3, Elastic Modulus of 16 MPa, Poisson's Ratio of 0.5, Tension of 10 GPa and no Friction Angle nor Dilation Angle. The tension ratio of 10 GPa is set this large to ensure that the failure of the model is due purely to shear failure and not in tension. The chosen material was characteristically comprised of relatively high cohesion and zero friction angles allowing it to have stable unsupported capabilities.

Having made the decision to include the pressure ratio, a large number of runs were conducted for each depth ratio while varying the strength ratios. For each depth ratio there were over 150 cases completed to provide the necessary data for analysis. With the speed of current computers it was possible to generate this large quantity of data. Elemental principal stresses, shear stain rates, velocity vectors, Y-displacements and plasticity indicators are to be plotted and discussed.

Within FLAC is a programming language known as FISH that gives the user the ability to define new variables and functions. These functions may be utilised to enhance the usefulness of FLAC through the application of these user defined features.

Sometimes FLAC's built-in grid generators will not be able to produce a desired geometry. A series of INITIAL commands can always be used to specify locations of individual grid points if all else fail. This can be tedious if every x- and y-point must be specified individually, but it is often possible to write a program that generates the grid automatically using the built-in programming language, FISH. (ITASCA Consulting Group 2014)

Within this investigation the FISH programming language is utilised to generate the required grid to simulate the geometry and geology of the region surrounding the trapdoor collapse. The FISH script designed as part of this investigation for the Tunnelling research group, of which this thesis is a product. The script sets the soil properties, mesh size and geometry of half a trapdoor scenario.

5.3 Analysis of Changing Pressure Ratios

Considering that the factor of safety is now dependent upon the three variables mentioned previously, an analysis was conducted in an attempt to determine the effect of each variable independently.

In the previous chapter, the pressure ratio was assumed to equal zero. Figure 27 is an example that illustrates the effect of changing pressure ratios. This particular example illustrates the effect when the depth ratio is equal to 6 and the strength ratio is equal to 1.

From Figure 27 when the pressure ratio was equal to zero as it was in the previous chapter, the factor of safety was approximately equal to 1. This result is comparable to the stability chart constructed in previously in chapter 4 and

reproduced as figure 28. The interpolated value for the factor of safety obtained from the stability chart can be seen to be approximately equal to 1.

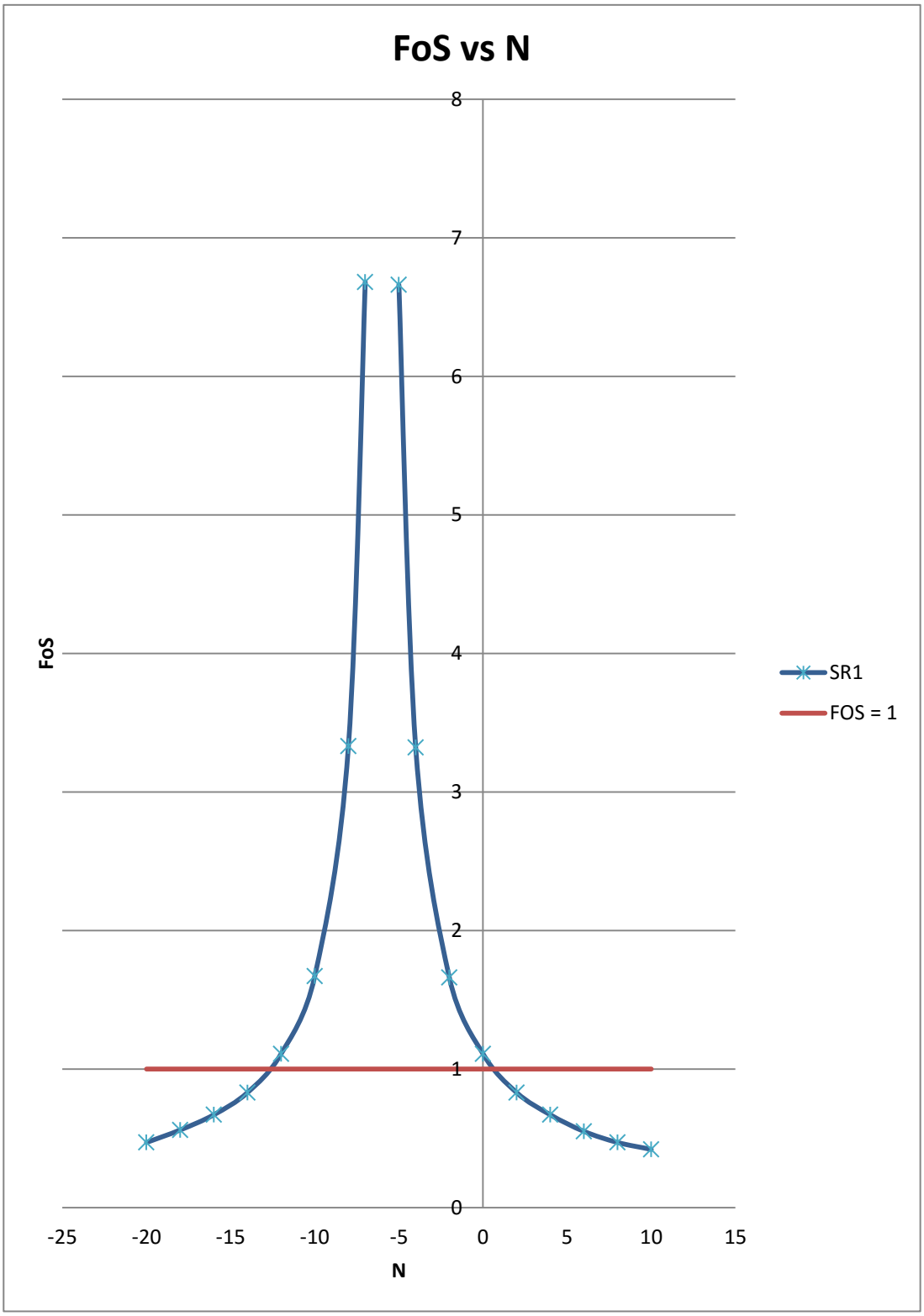

Figure 27 – Factor of Safety vs Pressure Ratio (HW=6 and SR=1)

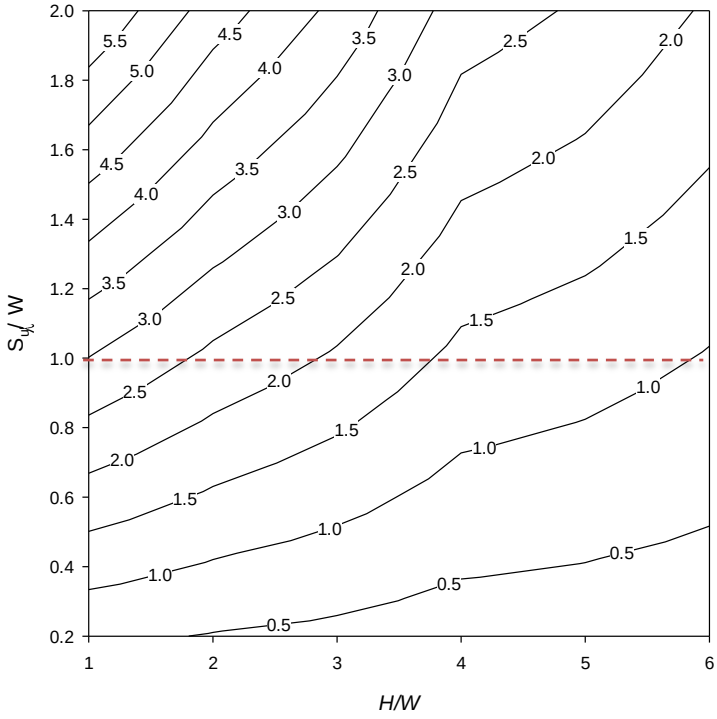

Figure 28 - Stability chart for *FoS* with respect to *H/W* and $S_u/\gamma W$

This plot of FoS vs N in figure 27 can be interpreted by considering the four stages demonstrating the different outcomes for the varying pressure ratios. The four stages are labelled stage 1 to 4.These stages can be visually understood by observing the velocity vectors for each stage.

Stage 1 is any scenario where the surcharge is greater than the internal pressure beneath the overburdening soil. This results in a positive pressure ratio. In these cases, failure will be a collapse failure of the overburdening soil due to unstable situations once the factor of safety becomes less than 1.

For this particular case stage 1 occurs when a positive pressure ratio exists. As the positive pressure ratio increases from zero, the factor of safety begins to decrease slowly resulting in more unstable conditions. The Velocity Plot shown in Figure 29 for Stage 1 clearly indicates that the overburden is in collapse due to the direction of the velocity vectors in the downwards direction.

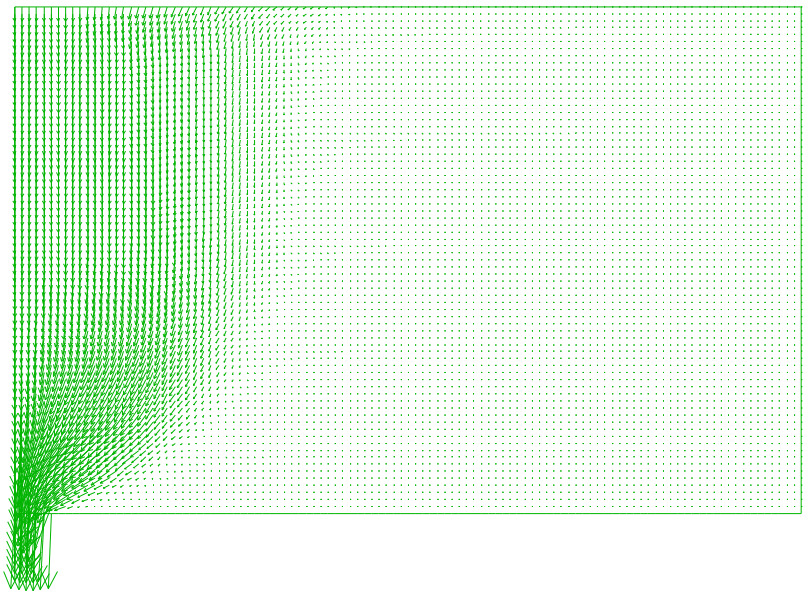

Figure 29 – Stage 1 Velocity Plot

Stage 2 occurs under the condition where the internal pressure is greater that the applied surcharge, however, the scenario is considered stable as results are achieving factors of safety greater than 1. The shear strength reduction method reduces the overburdening soil shear strength until a failure occurs. Looking at figure 27 it can be seen that in this stage, again, the failure will still be a collapse of the overburdening soil. As the pressure ratio N decreases (increase in negative pressure) the factor of safety increases sharply with a relatively small change in the pressure ratio.

It is assumed that the factor of safety in this stage will continue to increase until reaching an apparent maximum factor of safety. This maximum point of stability can be referred to as the point of equilibrium. It is at this point that a weightlessness condition is said to be apparent in the overburdening soil as the shear strength reduction method will continue to reduce the shear strength but will never achieve a failure state, thus resulting in an infinite factor of safety.

The Velocity Plot shown in Figure 30 for Stage 2 indicates that the overburden is in collapse due to the direction of the velocity vectors in the downwards direction.

There are no noticeable differences in the velocity plots between stage one and stage two.

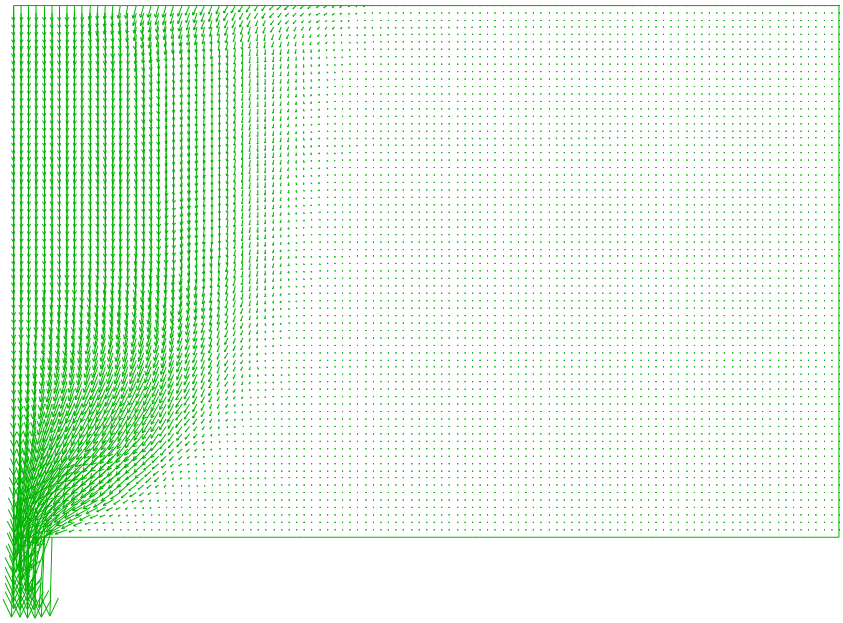

Figure 30 – Stage 2 Velocity Plot

Decreasing the pressure ratio further (increases in negative pressure) takes the model past the point of equilibrium into Stage 3 conditions. While still stable, the factor of safety quickly diminishes for small changes in the pressure ratio. This stage continues until a factor of safety of 1 is obtained. While the trapdoor is still considered stable, the internal pressure is increasing, relative to the surcharge, to the point of supporting the overburden as well as the applied surcharge load above the overburden.

The results in Stage 3 are now beginning to fail in an opposite sense. This means that the overburdening soil will experience a blowout scenario rather than a collapse. The Velocity Plot shown in Figure 31 for Stage 3 indicates that the overburden is about to blowout due to the direction of the velocity vectors in the upwards direction.

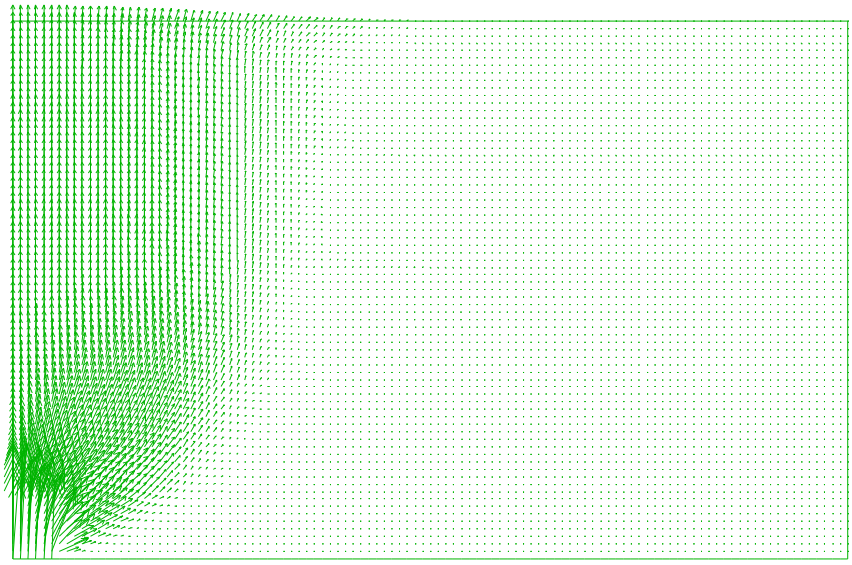

Figure 31 – Stage 3 Velocity Plot

Any further decrease in the pressure ratio takes the modelled scenario into the fourth and final stage. This is where the situation becomes unstable regardless of the soils strength ratio and fails due to blowout of the overburdening soil. The velocity plots in Figure 32 also demonstrate this as being the case.

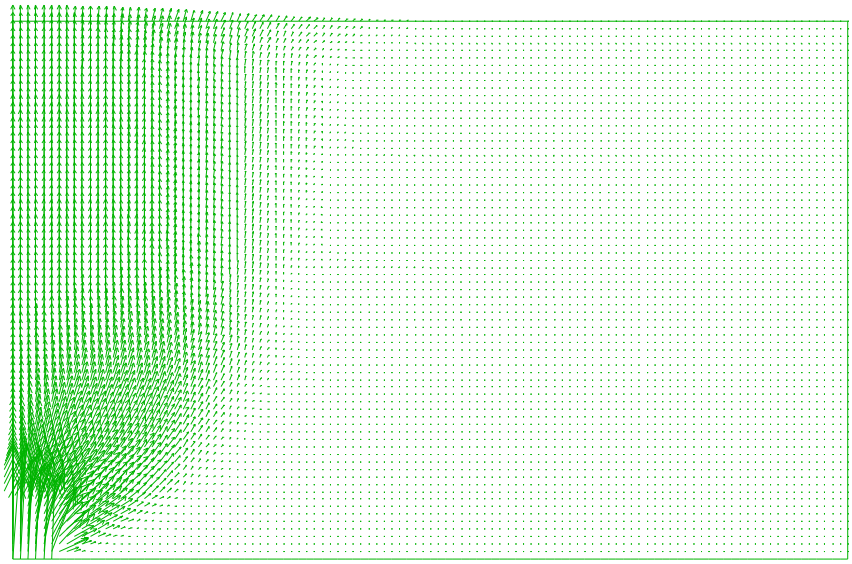

Figure 32 – Stage 4 Velocity Plot

5.4 Extent of Surface Failure due to Pressure Ratio

The depth ratio was found to have the most significant impact on the extent of surface failure. When the pressure ratio was assumed to be zero in chapter 4, the extent of these surface failures was illustrated in Figure 15 and recorded in table 3.

In comparison the shear strain rate plots are graphed below in figure 33 when the pressure ratio was kept at a constant of N = 2 and strength ratio of SR = 1.

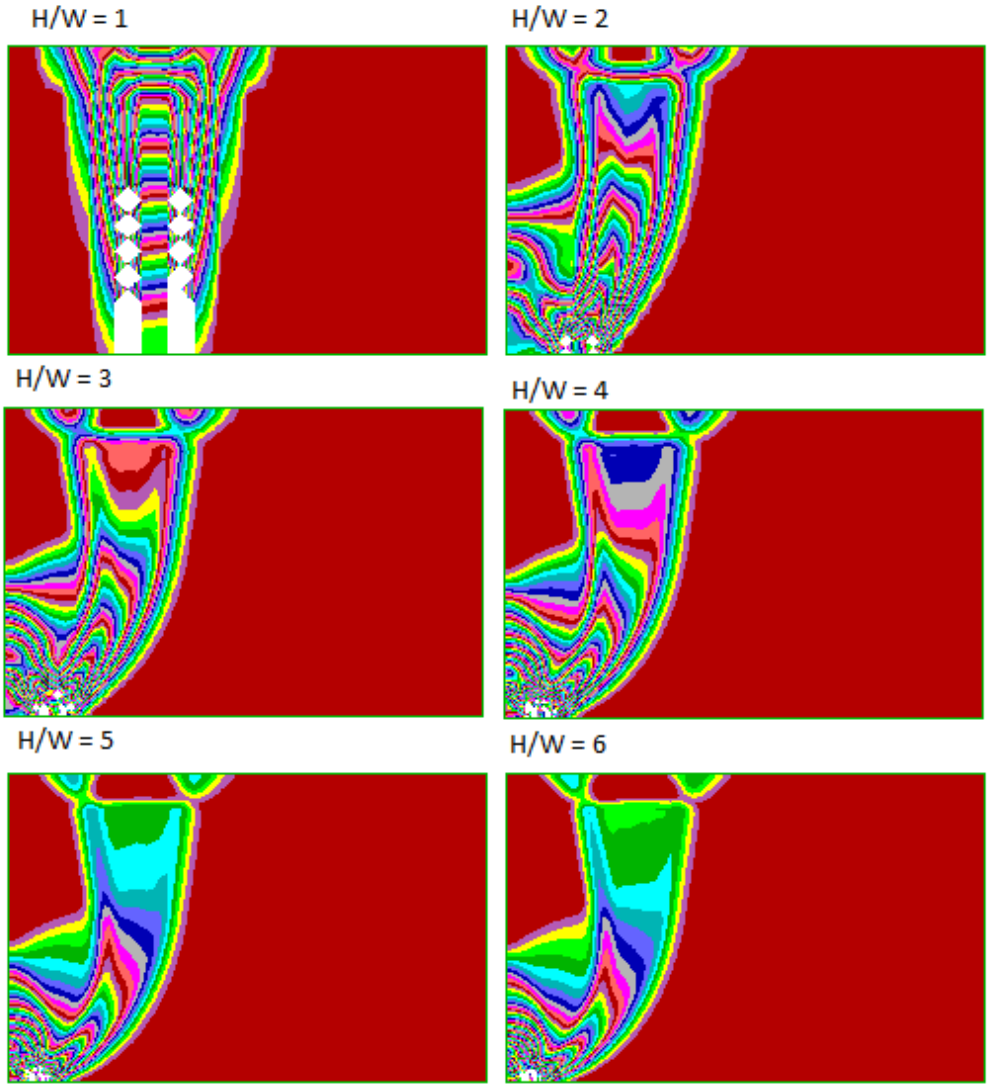

Figure 33 – Shear Strain Rate (SSR) Plots (SR=1, N=2)

Comparing figure 33 to figure 15 from chapter 4 it can be observed that there is a much greater change in shear strain rates with the increased pressure ratio. This is particuarly true the shallower the trapdoor is below the surface.

The collapse at the surface has also been affected due to the greater pressure ratio. There is a greater difference in the extent of the surface failure compared to the cavity width when the trapdoor is not as deep. These values are compared in table 3 below. As the depth ratio increases the two ratios are similar, particularly when the depth ratio was greater than 4. In chapter 4 soil arching was discussed and was more evident with the lower depth ratios. The increased pressure ratio due to a greater surcharge on the overburden is causing a greater arching effect and greater horizontal stain and soil movement.

Table 3 – Comparison of Surface Failure Ratios

Depth Ratio	Surface failure/Cavity Width N = 0	Surface failure/Cavity Width N = 2
1	1.60	1.70
2	2.87	3.03
3	4.27	4.43
4	5.70	5.87
5	7.10	7.13
6	8.50	8.50

5.5 Pressure Ratios with Varying Strength Ratios

The shape of the graph in figure 27 appears to be hyperbolic with the curve being asymptotic from both sides. This indicates the possibility of an infinite factor of safety being achieved which is unrealistic due to its own definition.

Using FLAC with a chosen mesh size of 0.5, results in apparent peaks for the FoS for any given strength ratio. These peak values may differ with a finer mesh size. The run-time restrictions of the smaller mesh make this difficult to perform in this investigation.

Combining the FoS vs N plots of all strength ratios for the given depth ratio of 2, as seen in figure 34, it is noticed that as the strength ratio decreases, meaning the undrained shear strength increases, the required pressure ratio to achieve a point of equilibrium decreases as the overburdening soil is more capable of supporting its self-weight.

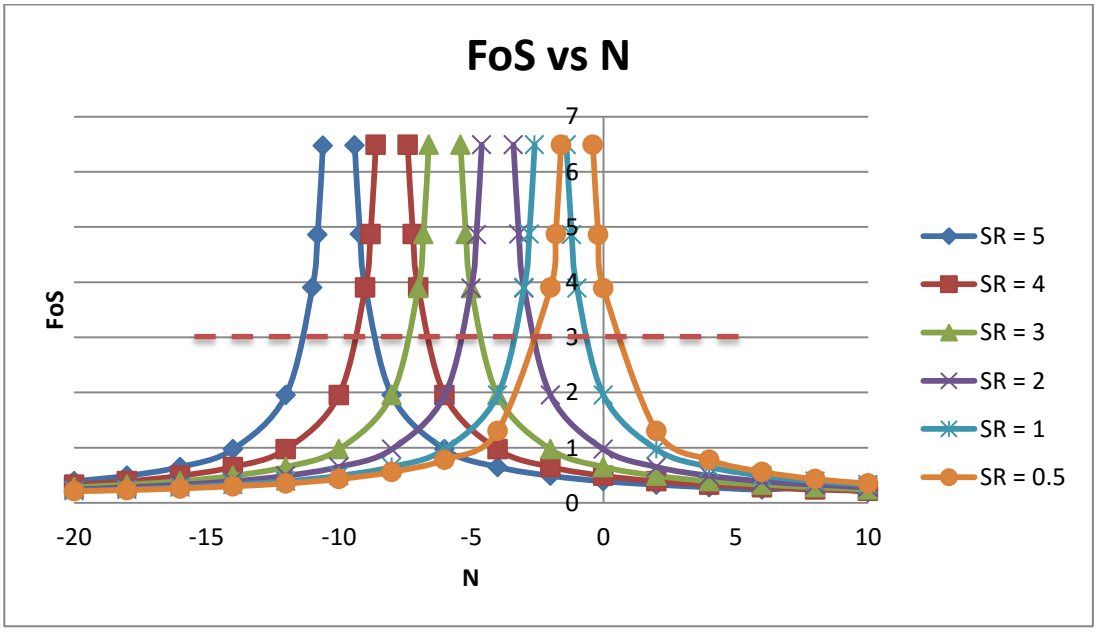

Figure 34 – Comparing Equilibrium points of each Strength ratio

By graphing these on the same axes it allows for the possibility of determining comparable ranges for the pressure ratios for differing strength ratios if a particular factor of safety is to be achieved. For example, if a factor of safety of 3 is required and the strength ratio was 5 then the pressure ratio required would be -8.5 and -11.5. These are the values for the pressure ratio for collapse and blowout failures respectively. Using a similar approach for a strength ratio of 0.5 gives the pressure ratios of 0.5 and -2.5 for collapse and blowout under these conditions.

As sinkholes are generally formed when collapse failure occurs rather than blowout failure, figure 35 is the same graph showing only these collapse branches to simplify the plot. Using this figure it would only be able to determine the results for the more common collapse failure conditions.

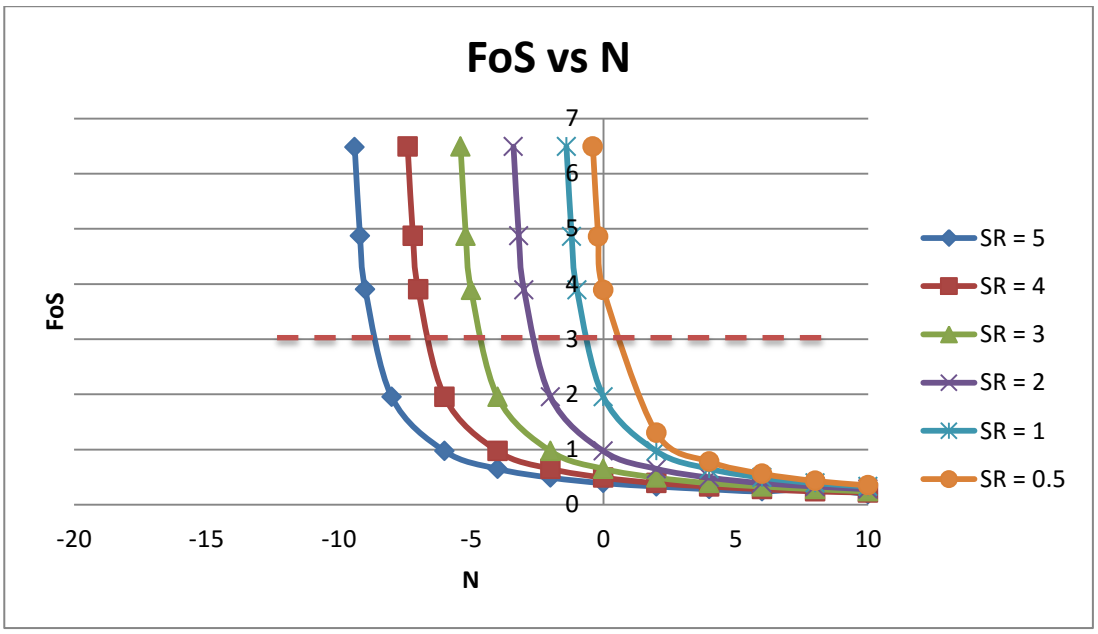

Figure 35 – Comparing Equilibrium points of each Strength ratio

5.6 Critical Pressure and Strength Ratios

Another approach is to investigate the critical strength and pressure ratios. These can be conveniently converted from both the strength and pressure ratios by multiplying both by the Factor of Safety. These are the dimensionless strength and pressure ratio which maintain stability (FoS = 1). These results are directly comparable to those from Wilson et al. (2011), which used finite element

formulations of limit theorems as described by Lyamin (2002) and Kraennemhoft (2005, 2007). Safe limits for stability or pressure ratios are found by using the lower bound theorem. Then conservative estimates for the pressure ratio were found by the upper bound theorem. The true solution lies within these upper and lower values and is used to validate these results.

The Critical values are defined as equations:

$$Critical\ Pressure\ Ratio\ (N_c) = \frac{\sigma_s - \sigma_t}{S_u}.FoS$$

$$Critical\ Strength\ Ratio\ (SR)_c = \frac{\gamma W}{S_u}.FoS$$

Having adjusted the strength and pressure ratios to obtain these critical values, the data was plotted for each strength ratio. An example of these plots can be seen in figure 36.

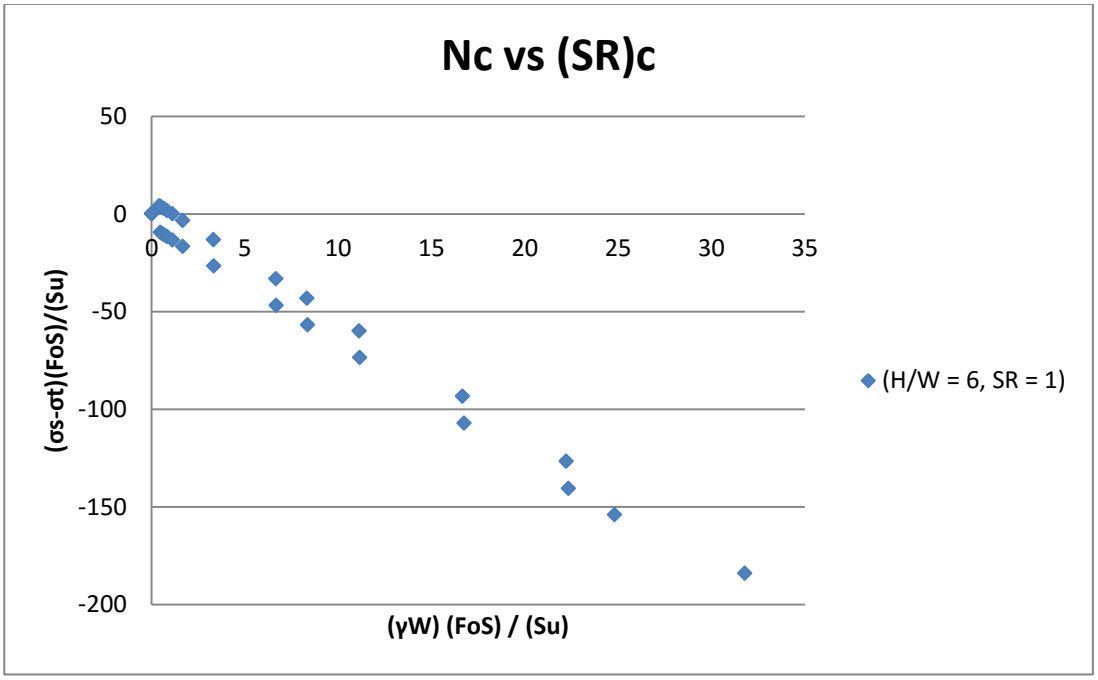

Figure 36 – Critical Pressure and Strength Ratio

The difference between blowout and collapse of the overburdening soil is possible to be interpreted from this graph by the two converging trends that are meeting at the equilibrium position. The upper trend indicates the collapse failure whereas the

lower trend indicates the blowout conditions. Each of these plots for differing depths ratios were compiled and plotted against each other for ease of comparison, seen in figure 37 below.

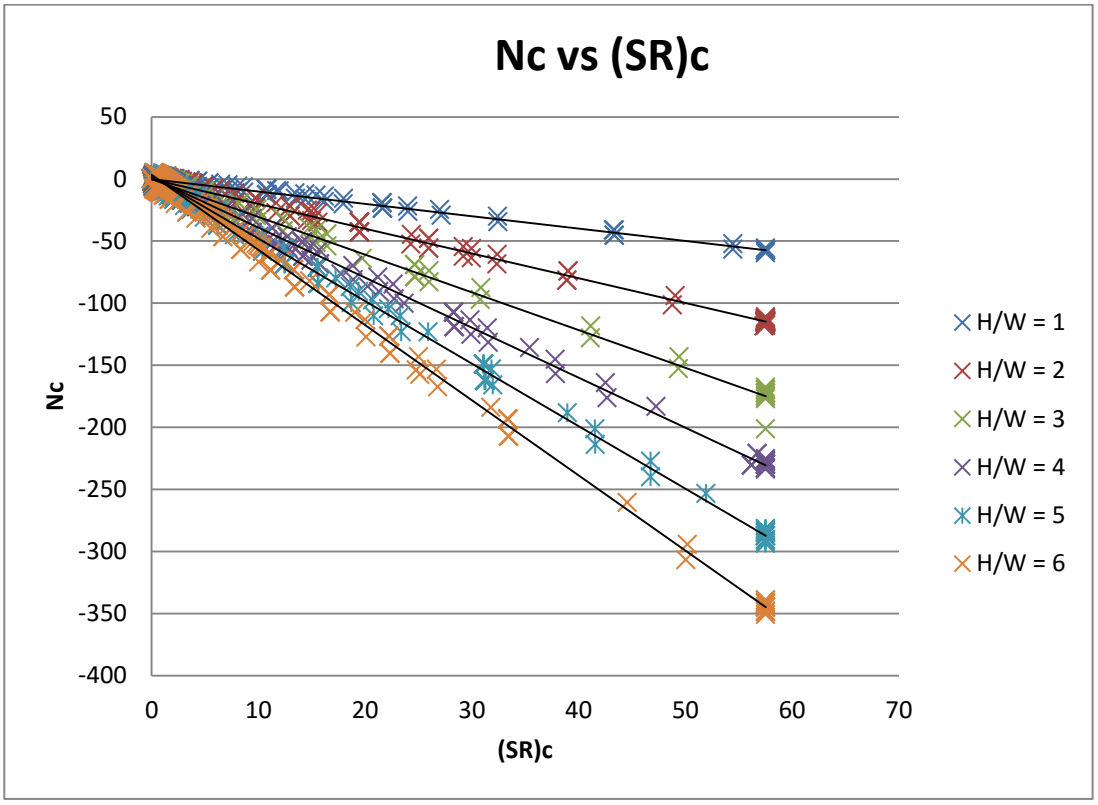

Figure 37 – Stability Chart of Critical Data at different Depth ratios

Due to the large range of pressure ratios, the data can be plotted in two separate graphs. The graph in figure 38 represents depth ratios 1 to 3 and figure 39 shows the depth ratios 4 to 6.

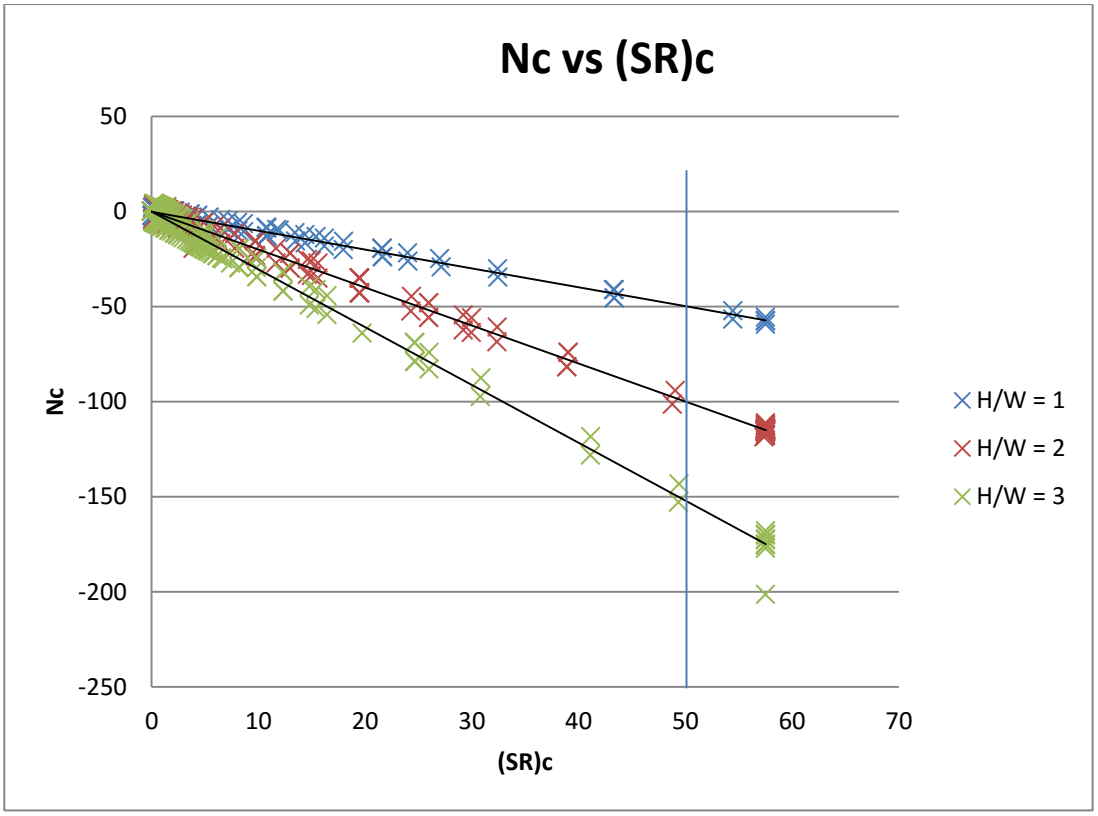

Figure 38 – Stability Chart for Depth Ratios 1 to 3

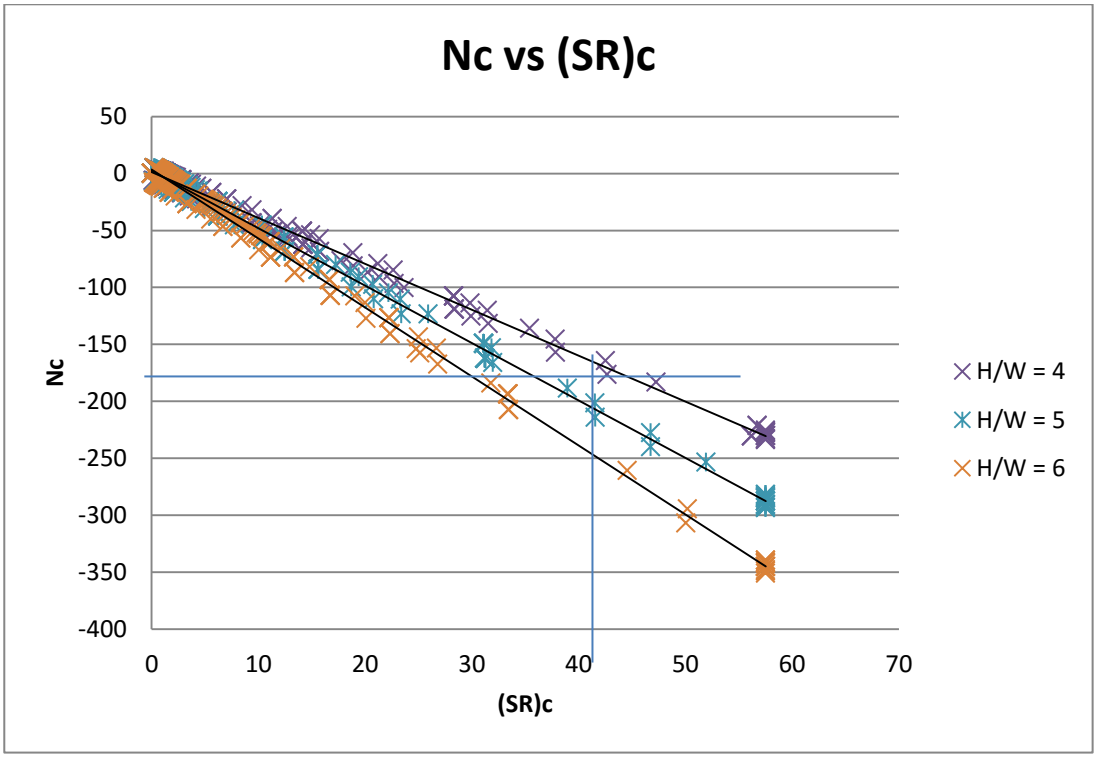

Figure 39 – Stability Chart for Depth Ratios 4-6

These plots indicate a direct proportion between the critical pressure and strength ratios. The constant of proportionality was determined and tabulated in table 4 below.

Table 4 – Proportionality Constants

H/W	k	Approximate Gradient
1	-0.994	-1
2	-1.998	-2
3	-3.039	-3
4	-4.032	-4
5	-5.042	-5
6	-6.059	-6

The gradients of each trend, the constant of proportionality, suggest that it is linked to the negative corresponding depth ratio. This suggests that the gradient of each line is equal to $-\frac{H}{W}$.

Therefore:

$$y = kx$$

Substituting for the Critical Pressure and Strength along with the gradient gives:

$$\frac{\sigma_s - \sigma_t}{S_u}.FoS = -\left(\frac{H}{W}\right)\frac{\gamma W}{S_u}.FoS \quad (5.8)$$

Cancelling out simplifies equation to:

$$\sigma_s - \sigma_t = -H\gamma \quad (5.9)$$

This simplified equation proposes the difference in pressure is directly proportional to the depth depending on the soil cohesiveness. This can be interpreted that a deeper sinkhole requires a greater change in pressure to maintain stability for any given soil body.

5.7 Stability Chart and Practical Uses

These stability charts may be used to quickly interpolate to find one of the following: the critical strength ratio, critical pressure ratio or depth ratio. In all cases these will be critical values since these charts are working on a factor of safety of 1.

For example, using Figure 38 with the scenario of a strength ratio of 50 and a depth ratio of 3 and interpolating to approximate the pressure ratio to be -155. This can be compared to results using the equation by substituting in the values

$$\frac{\sigma_s - \sigma_t}{S_u}.FoS = -\left(\frac{H}{W}\right)\frac{\gamma W}{S_u}.FoS$$

$$\frac{\sigma_s - \sigma_t}{S_u}.FoS = -(3) \times 50 \times 1$$

$$\frac{\sigma_s - \sigma_t}{S_u}.FoS = -150$$

Another example could be using a known critical pressure ratio -180 with a known critical strength ratio of 42 to interpolate the depth ratio for critical stability conditions. Using figure 39 and the known values an approximate depth ratio of 4.3 is obtained. Comparing this with equation 5.8

$$-180 = -\left(\frac{H}{W}\right) \times 42$$

$$\left(\frac{H}{W}\right) = 4.28$$

The stability charts simplify the process and give accurate but not precise value for any critical situation.

5.8 Comparison of Results

Previous investigation into critical values for pressure ratios and strength ratios where conducted by (Wilson 2011). This study investigated the undrained stability where shear strength increased linearly with depth.

Wilson et al. generated data for critical strength ratios up to five. In the FLAC simulation undertaken in this thesis the critical strength ratio has been calculated to be as large as sixty. The results of this investigation are compared to Wilson's data. The plots from figure 37 where restricted to critical strength ratios between zero and five shown below in figure 40 along with Lower and Upper values of critical pressure ratios obtained from Wilsons investigation.

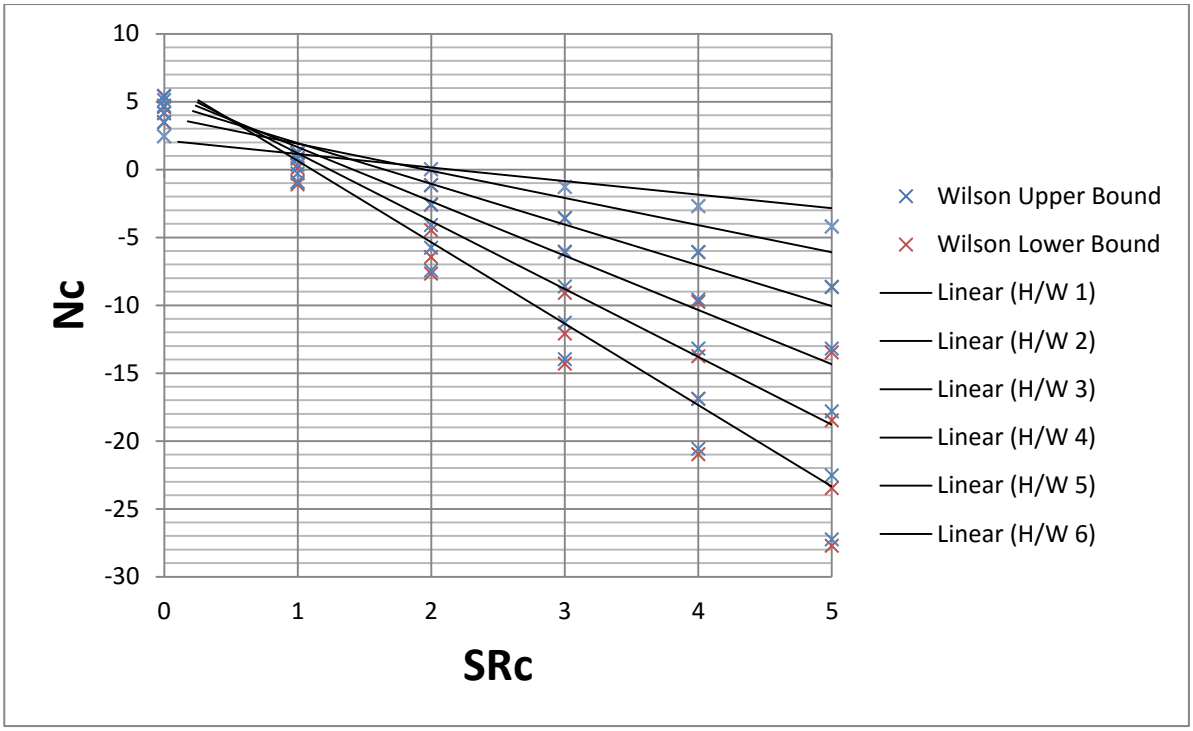

Figure 40 – Stability Chart of Critical Data at different Depth ratios

The data obtained from the shear strength reduction using FLAC follows the same general trends; however, it seems to be underestimating the critical pressure ratios

and lie outside the upper and lower bounds obtained by Wilsons study into tunnels.

Two possible causes for these differences could be the difference between investigating tunnels as opposed to the trapdoor scenario and that Wilson was increasing the shear strength linearly with the depth of the tunnel. Further research into other sources of data to compare the results obtained will need to be conducted to justify the results obtained from this modelling.

Chapter 6

6.1 Outcomes of Modelling

This project assisted in further understanding how sinkhole development can be analysed through analytical theories and the application of numerical methods to create simulations.

The analysis was conducted through the use of the software program Fast Lagrangian Analysis of Continua (FLAC). The 2D numerical models were used to generate factors of safety through the shear strength reduction method of many trapdoors under varying depth, pressure and strength of material properties and different overburden depth to cavity width ratios.

When purely cohesive homogenous undrained clay was tested under zero pressure ratio conditions and constant shear strength ratio the effect on the extent of the surface failure was significant with the changing depth ratio. The relationship was linear with a strong correlation. The data also indicates that the shallower the trapdoor of the sinkhole, the greater the effect of soil arching throughout the overburdening clay.

For a fixed depth ratio increasing the soils strength ratio by up to a factor of 10 had minimal effect on the extent of surface failure as evident by the similar slip planes for these test.

In terms of stability, the factor of safety was found to be directly proportional to the strength ratio of the soil for a given depth ratio. The factor of safety was also found to be to be inversely proportional to the depth ratio for a given strength ratio. Therefore under zero external pressure the factor of safety is a function of depth ratio and strength ratio, $FOS = f\left(\frac{H}{W}, \frac{\gamma W}{S_u}\right)$.

Stability charts formed from the data produced from the shear strength reduction method using FLAC were found to be accurate and a useful practical aide to quickly determine an approximate level of stability. These stability charts correlated

strongly with the proposed stability equations and may therefore in future be utilised.

The many varying cases with regards to surcharge pressure and internal pressure within the cavity where tested to determine to what extent the pressure ratio affected the resulting sinkhole formed under these varying pressure conditions. These investigations of the effect of changing pressure ratios produce plots that clearly demonstrated the two cases of sinkhole collapse and sinkhole blowout failure.

With respect to the extent surface failure, the increasing pressure ratios had a noticeable difference for shallow sinkholes. When compared to zero pressure outcomes, as the depth ratio increased so that the overburden was five to six times larger than the width of the sinkhole, the increased pressure ratio caused minimal to no changes to the extent of the resulting hole at the surface.

The investigation into critical pressure and strength ratios has led to the creation of Critical Stability charts. These charts are critical as the factor of safety value is equal to one and hence these charts may be used in all cases. These again may be useful resources upon further development and testing. Further analysis of these plots has indicated that the difference between the surcharge pressure of the overburden soil and the internal pressure within the sinkhole cavity is largely dependent upon the depth of the sinkhole and the soil cohesion.

6.2 Recommendations

The outcomes of this investigation have been based on purely cohesive homogenous undrained clay, following the recommendations suggested in the work of Brian Lamb (2014). All findings under any pressure ratio appear to be dependent upon the depth or depth ratio of the cavity opening more than any other contributing factor.

Considering that this investigation kept a constant width, therefore any change in depth ratio was due to the change in depth, a further investigation into depth ratio should consider changes to both width and depth to clarify if it is the depth ratio or the depth that is the main factor affecting the size of sinkhole collapse.

Working in a 2 dimensional space simplifies the model and reduces the runtime of computer simulations. A possible future development would be to further any FLAC investigation into factors contributing to sinkhole formation to include 3 dimensional analysis.

In reality the overburdening soil could be made up of differing layers of overburden material. Simulating this complicates the computer modelling however; further investigation into this more realistic situation may be beneficial.

References

Augarde et al., CA, L Sloan, S 2003, 'Stability of an undrained plane strain heading revisited', *Computers and Geotechnics 30*, pp. 419–30.

Baryakh, A, A. K. 2001, 'Sinkhole Formation Mechanism', *Journal of Mining Science*, vol. vol. 47, no. no. 4.

Bishop, A 1955, 'The use of slip circle in the stability analysis of slopes', *Geotechnique*, vol. vol. 5(1), pp. 7-17.

Blom, Ja 2013, *That Sinking Feeling*, <http://www.jpl.nasa.gov/news/news.php?release=2014-073>.

Budetta, GaDN, C 1995, 'Magnetic field changes on lava flow to detect lave tubes.', *Journal of Vocanology Geothermal Research*, vol. 65, pp. 237-48.

Cala .M, JFAT 2004, 'Slope stability analysis with modified shear strength reduction technique', *Dept. of Geomechanics, Civil Engineering & Geotechnics, AGH University of Science & Technology, Poland*.

Corne, B 2014, 'sinkhole: Precursory deformation measured by radar interferometry Geology', vol. v. 42, no. 111-114.

Davis, E, Gunn, MJ, Mair, RJ & Seneviratne, HN 1980, 'The stability of shallow tunnels and underground openings in cohesive material', *Geotechnique*, vol. vol. 30 (4), pp. 397-416.

Dill, RF 1977, 'The blue holes, geologically significant submerged sinkholes and caves off British Honduras and Andros, Bahama Islands.', *Proc. 3rd Int. Reef Symp., 2,*, pp. 237–42.

Ford, DaW, P 1989, 'Karst Geomorphology and Hydrology', *Unwin Hyman Ltd*.

Gischler, FSA, Eugene A. Shinnc 2013, 'Seismic stratigraphy of the Blue Hole (Lighthouse Reef, Belize), a late Holocene climate and storm archive', *Marine Geology*, vol. 344, pp. 155–62.

Group, IC 2011, 'I FLAC Fast Lagrangian Analysis of Continua Online Manual'.

Group, IC 2014, 'FLAC Advanced', *Two Dimensional Continuum Modeling for Geotechnical Analysis of Rock, Soil, and Structural Support*.

Gutiérrez, F, J.P Guerrero, J Lucha, P Cendrero, A Remondo, J Bonachea, J Gutiérrez, M Sánchez, J.A 2006, 'The origin, typology, spatial distribution and detrimental effects of the sinkholes developed in the alluvial evaporite karst of the Ebro River valley downstream of Zaragoza city (NE Spain)', *EARTH SURFACE PROCESSES AND LANDFORMS*, vol. vol. 32, pp. 912-28.

Lamb, B 2014, 'A Physical and Numerical Investigation into Sinkhole Formation'.

Land, L 2013, 'Integrating Science and Engineering to Solve Karst Problems', *The 13th Multidisciplinary Conference on Sinkholes and the Engineering & Environmental Impacts of Karst*.

Lei, M, Y Jiang, X 2005, 'Experimental Study of Physical Models for Sinkhole Collapses in Wuhan, China', *Sinkholes and the Engineering and Environmental Impacts of Karst*.

Lyamin, A, & Sloan, SW 2002, 'Lower bound limit analysis using non-linear programming', *International Journal for Numerical Methods in Engineering*, vol. vol. 55, no. no. 5, pp. 573-611.

Manger et al., J 1986, 'A water treatment/disposal site evaluation process for areas underlain by carbonate aquifers', *Round Water Monitoring Review*, vol. 6:2, pp. pp. 117 – 21.

Marini, A, F Healey, S n.d, 'Three Dimensional Modelling for Sinkhole Analysis in the Mining Area of Acquaresi', *Earth Science Dept University of Cagliari*.

Mining, Bo 2006, 'Potential Impacts from Underground Mining', *Pennsylvania Department of Environmental Protection*.

Neubert, B, J.A Xueming, Xu et al 2008, '3-D Photo Real Modeling of Devil's Sinkhole in Rocksprings', *Sinkholes and the Engineering and Environmental Impacts of Karst*.

Otter, J, Cassell, AC & Hobbs, R E 1966, 'Dynamic relaxation', *Proceedings of the Institution of Civil Engineers*, vol. Vol: 35, no. 633-656.

Radoslaw L. Michalowski, F 2002, 'Stability Charts for Uniform Slopes', *JOURNAL OF GEOTECHNICAL AND GEOENVIRONMENTAL ENGINEERING*.

RAINES, TW 1968, 'Sotano de las Golondrinas', *Association for Mexican Cave Studies*, vol. BULLETIN 2.

Satarugsa, P 2011, 'The Lessons Learnt from Geophysical Investigation of Sinkholes in Rock Salt in Thailand ', *nternational Conference on Geology, Geotechnology and Mineral Resources of Indochin*.

Sloan et al., SW, Assadi, A., Purushothaman, N 1990, 'Undrained stability of a trapdoor', *Geotechnique*, vol. 40, no. 1, pp. 45-62.

Sowers, GF 1996, *Building on Sinkholes: Design and Construction of Foundations in Karst Terrain*.

Taylor, D 1937, 'Stability of earth slopes', *Journal of the Boston Society of Civil Engineers*, vol. vol. 24, no. no. 3, pp. 197-246.

V.Hutton 2004, 'Fundamental of Finite Element Analysis', *McGraw-Hill*.

Warren, WM 1974, 'Retention Basin Failures. Carbonate Terrains.', *Water Resource Bulletin*, vol. 10, no. 1.

Weihai, ZXaC n.d, 'Tiankengs in the karst of China', *Speleogenesis and Evolution of Karst Aquifers*, no. 1814-294X.

Wilson, D, Abbo, AJ, Sloan, SW, Lyamin & AV 2011, 'Undrained stability of a circular tunnel where the shear strength increase linearly with depth', *Canadian Geotechnical Journal*, vol. vol. 48, pp. 1328-42.

Appendices

Appendix A: Project Specification

FACULTY OF ENGINEERING AND BUILT ENVIRONMENT

ENG 4111/4112 Research Project

Project Specification

FOR:	**Anthony Keightley**
TOPIC:	Three Dimensional Investigation into Sinkhole deformation
SUPERVIOSR:	Dr. Jim Shiau
ENROLMENT:	ENG 4111 – S1 2015 ENG 4112 – S2 2015
PROJECT AIM:	Investigating further into the predicted behaviour of the formation of Sinkholes, predominately focusing on 3D Numerical Modelling.
SPONSORSHIP:	USQ
PROGRAMME:	**Issue A, 18/03/2015**

1. Introduction – General information on project including procedure/methodology of the paper
2. Introduction to technical information and case studies of existing sinkholes eg. Trapdoor Theory
3. Explanation of Flac to gain an understanding of how the program works
4. 2D model generation and refinement of existing 2D models
    a. Investigating undrained clay, possibly c - Ø
5. 3D model generation with investigation into differing trapdoor shapes and there effects on the deformation and final sinkhole shape
6. Conclusion and future work

This Project Specification does not reflect the final thesis document, as it has changed greatly over the course of the year due to the advice and recommendations from my supervisor Dr Jim Shiau.

Appendix B: Summary Table

Location	Description	Diameter Information	Depth Information
China	Tiankengs "skyholes" Double Nested Structure (Natural)	581.5m average	331m average
America	Brine Well Collapse (Human origin)	111m approximately	45m
Mexico	Cave Shaft (Natural)	Upper 55m average Lower 218.5m average	351.5m average
Australia	(Natural)	N/A	N/A
Central America	Reefal Karst Cavity (Natural)	320m average	125m average

Appendix C: Raw Data N = 0

H/W	H	SR =(γW)/Su	Su (kPa)	FLAC FoS
1	6	0.2	21.6	0.43
1	6	0.4	43.2	0.86
1	6	0.6	64.8	1.29
1	6	0.8	86.4	1.72
1	6	1	108	2.16
1	6	1.3	140.4	2.80
1	6	1.6	172.8	3.45
1	6	2	216	4.31
2	12	0.2	21.6	0.39
2	12	0.4	43.2	0.78
2	12	0.6	64.8	1.17
2	12	0.8	86.4	1.56
2	12	1	108	1.95
2	12	1.3	140.4	2.53
2	12	1.6	172.8	3.11
2	12	2	216	3.89
3	18	0.2	21.6	0.33
3	18	0.4	43.2	0.66
3	18	0.6	64.8	0.99
3	18	0.8	86.4	1.31
3	18	1	108	1.64
3	18	1.3	140.4	2.13
3	18	1.6	172.8	2.63
3	18	2	216	3.28
4	24	0.2	21.6	0.28
4	24	0.4	43.2	0.56
4	24	0.6	64.8	0.85
4	24	0.8	86.4	1.13
4	24	1	108	1.41
4	24	1.3	140.4	1.83
4	24	1.6	172.8	2.26
4	24	2	216	2.82
5	30	0.2	21.6	0.25
5	30	0.4	43.2	0.50
5	30	0.6	64.8	0.74
5	30	0.8	86.4	0.99
5	30	1	108	1.24

5	30	1.3	140.4	1.61
5	30	1.6	172.8	1.99
5	30	2	216	2.48
6	36	0.2	21.6	0.22
6	36	0.4	43.2	0.44
6	36	0.6	64.8	0.67
6	36	0.8	86.4	0.89
6	36	1	108	1.11
6	36	1.3	140.4	1.44
6	36	1.6	172.8	1.76
6	36	2	216	2.22

Appendix D: Raw Data N ≠ 0 (H/W = 6)

SR =(γW) / Su (1)	Su (kPa)	N=(σs-σt)/Su (2)	σs (Kpa)	FLAC FoS (3)	Critical Strength Ratio =(γW) (FoS) / (Su) -- when FoS=1	Critical Stability Number N=(σs-σt)(FoS)/(Su) -- when FoS=1
5	21.6	-33	-712.8	2.23	11.15	-73.59
5	21.6	-32	-691.2	3.35	16.75	-107.2
5	21.6	-31	-669.6	6.69	33.45	-207.39
5	21.6	-30	-648	11.5	57.5	-345
5	21.6	-29	-626.4	6.68	33.4	-193.72
5	21.6	-28	-604.8	3.33	16.65	-93.24
5	21.6	-27	-583.2	2.22	11.1	-59.94
5	21.6	-26.8	-578.88	2.08	10.4	-55.744
5	21.6	-26.6	-574.56	1.96	9.8	-52.136
5	21.6	-26.4	-570.24	1.85	9.25	-48.84
5	21.6	-26.2	-565.92	1.75	8.75	-45.85
5	21.6	-26	-561.6	1.67	8.35	-43.42
5	21.6	-25.8	-557.28	1.58	7.9	-40.764
5	21.6	-25.6	-552.96	1.51	7.55	-38.656
5	21.6	-25.4	-548.64	1.45	7.25	-36.83
5	21.6	-25.2	-544.32	1.39	6.95	-35.028
5	21.6	-25	-540	1	5	-25
5	21.6	-24.8	-535.68	1.28	6.4	-31.744
5	21.6	-24.6	-531.36	1.23	6.15	-30.258
5	21.6	-24.4	-527.04	1.19	5.95	-29.036
5	21.6	-24.2	-522.72	1.15	5.75	-27.83
5	21.6	-24	-518.4	1.11	5.55	-26.64
5	21.6	-23.8	-514.08	1.07	5.35	-25.466

5	21.6	-23.6	-509.76	1.04	5.2	-24.544
5	21.6	-23.4	-505.44	1.01	5.05	-23.634
5	21.6	-23.2	-501.12	0.98	4.9	-22.736
5	21.6	-22	-475.2	0.83	4.15	-18.26
5	21.6	-20	-432	0.67	3.35	-13.4
5	21.6	-18	-388.8	0.55	2.75	-9.9
5	21.6	-16	-345.6	0.47	2.35	-7.52
5	21.6	-14	-302.4	0.42	2.1	-5.88
5	21.6	-12	-259.2	0.37	1.85	-4.44
5	21.6	-10	-216	0.33	1.65	-3.3
5	21.6	-8	-172.8	0.3	1.5	-2.4
5	21.6	-6	-129.6	0.28	1.4	-1.68
5	21.6	-4	-86.4	0.26	1.3	-1.04
5	21.6	-2	-43.2	0.24	1.2	-0.48
5	21.6	0	0	0.22	1.1	0
5	21.6	2	43.2	0.21	1.05	0.42
5	21.6	4	86.4	0.2	1	0.8
5	21.6	6	129.6	0.19	0.95	1.14
5	21.6	8	172.8	0.17	0.85	1.36
5	21.6	10	216	0.17	0.85	1.7

4	27	-26	-702	3.35	13.4	-87.1
4	27	-25	-675	6.7	26.8	-167.5
4	27	-24	-648	14.38	57.52	-345.12
4	27	-23.8	-642.6	14.38	57.52	-342.244

4	27	-23.6	-637.2	14.38	57.52	-339.368
4	27	-23.4	-631.8	11.14	44.56	-260.676
4	27	-23.2	-626.4	8.35	33.4	-193.72
4	27	-23	-621	6.67	26.68	-153.41
4	27	-22.8	-615.6	5.56	22.24	-126.768
4	27	-22.6	-610.2	4.76	19.04	-107.576
4	27	-22.4	-604.8	4.17	16.68	-93.408
4	27	-22.2	-599.4	3.7	14.8	-82.14
4	27	-22	-594	3.33	13.32	-73.26
4	27	-21.8	-588.6	3.03	12.12	-66.054
4	27	-21.6	-583.2	2.78	11.12	-60.048
4	27	-21.4	-577.8	2.56	10.24	-54.784
4	27	-21.2	-572.4	2.38	9.52	-50.456
4	27	-20	-540	1.67	6.68	-33.4
4	27	-18	-486	1.11	4.44	-19.98
4	27	-16	-432	0.83	3.32	-13.28
4	27	-14	-378	0.67	2.68	-9.38
4	27	-12	-324	0.55	2.2	-6.6
4	27	-10	-270	0.47	1.88	-4.7
4	27	-8	-216	0.42	1.68	-3.36
4	27	-6	-162	0.37	1.48	-2.22
4	27	-4	-108	0.33	1.32	-1.32
4	27	-2	-54	0.3	1.2	-0.6
4	27	0	0	0.28	1.12	0
4	27	2	54	0.26	1.04	0.52
4	27	4	108	0.24	0.96	0.96
4	27	6	162	0.22	0.88	1.32

4	27	8	216	0.21	0.84	1.68
4	27	10	270	0.2	0.8	2

3	36	-20	-720	3.35	10.05	-67
3	36	-19	-684	6.7	20.1	-127.3
3	36	-18.8	-676.8	8.38	25.14	-157.544
3	36	-18.6	-669.6	11.15	33.45	-207.39
3	36	-18.4	-662.4	16.68	50.04	-306.912
3	36	-18.2	-655.2	19.17	57.51	-348.894
3	36	-18	-648	19.17	57.51	-345.06
3	36	-17.8	-640.8	19.17	57.51	-341.226
3	36	-17.6	-633.6	16.73	50.19	-294.448
3	36	-17.4	-626.4	11.12	33.36	-193.488
3	36	-17.2	-619.2	8.34	25.02	-143.448
3	36	-17	-612	6.67	20.01	-113.39
3	36	-16	-576	3.33	9.99	-53.28
3	36	-14	-504	1.66	4.98	-23.24
3	36	-12	-432	1.11	3.33	-13.32
3	36	-10	-360	0.83	2.49	-8.3
3	36	-8	-288	0.67	2.01	-5.36
3	36	-6	-216	0.55	1.65	-3.3
3	36	-4	-144	0.47	1.41	-1.88
3	36	-2	-72	0.42	1.26	-0.84
3	36	0	0	0.37	1.11	0
3	36	2	72	0.33	0.99	0.66

3	36	4	144	0.3	0.9	1.2
3	36	6	216	0.28	0.84	1.68
3	36	8	288	0.26	0.78	2.08
3	36	10	360	0.24	0.72	2.4

2	54	-20	-1080	0.83	1.66	-16.6
2	54	-18	-972	1.11	2.22	-19.98
2	54	-16	-864	1.67	3.34	-26.72
2	54	-14	-756	3.34	6.68	-46.76
2	54	-13	-702	6.7	13.4	-87.1
2	54	-12.8	-691.2	8.37	16.74	-107.136
2	54	-12.6	-680.4	11.17	22.34	-140.742
2	54	-12.4	-669.6	16.73	33.46	-207.452
2	54	-12.2	-658.8	28.76	57.52	-350.872
2	54	-12.1	-653.4	28.76	57.52	-347.996
2	54	-12	-648	28.76	57.52	-345.12
2	54	-11.9	-642.6	28.76	57.52	-342.244
2	54	-11.8	-637.2	28.76	57.52	-339.368
2	54	-11.6	-626.4	16.69	33.38	-193.604
2	54	-11.4	-615.6	11.12	22.24	-126.768
2	54	-11.2	-604.8	8.33	16.66	-93.296
2	54	-11	-594	6.66	13.32	-73.26
2	54	-10	-540	3.33	6.66	-33.3
2	54	-8	-432	1.66	3.32	-13.28
2	54	-6	-324	1.11	2.22	-6.66

2	54	-4	-216	0.83	1.66	-3.32
2	54	-2	-108	0.67	1.34	-1.34
2	54	0	0	0.55	1.1	0
2	54	2	108	0.47	0.94	0.94
2	54	4	216	0.42	0.84	1.68
2	54	6	324	0.37	0.74	2.22
2	54	8	432	0.33	0.66	2.64
2	54	10	540	0.3	0.6	3

1	108	-20	-2160	0.47	0.47	-9.4
1	108	-18	-1944	0.56	0.56	-10.08
1	108	-16	-1728	0.67	0.67	-10.72
1	108	-14	-1512	0.83	0.83	-11.62
1	108	-12	-1296	1.11	1.11	-13.32
1	108	-10	-1080	1.67	1.67	-16.7
1	108	-8	-864	3.33	3.33	-26.64
1	108	-7	-756	6.68	6.68	-46.76
1	108	-6.8	-734.4	8.36	8.36	-56.848
1	108	-6.6	-712.8	11.15	11.15	-73.59
1	108	-6.4	-691.2	16.74	16.74	-107.136
1	108	-6.295	-679.86	22.34	22.34	-140.6303
1	108	-6.21	-670.68	24.8	24.8	-154.008
1	108	-6.2	-669.6		0	0
1	108	-6	-648		0	0
1	108	-5.8	-626.4		0	0

1	108	-5.79	-625.32	31.79	31.79	-184.0641
1	108	-5.7	-615.6	22.22	22.22	-126.654
1	108	-5.6	-604.8	16.66	16.66	-93.296
1	108	-5.4	-583.2	11.11	11.11	-59.994
1	108	-5.2	-561.6	8.32	8.32	-43.264
1	108	-5	-540	6.66	6.66	-33.3
1	108	-4	-432	3.32	3.32	-13.28
1	108	-2	-216	1.66	1.66	-3.32
1	108	0	0	1.11	1.11	0
1	108	2	216	0.83	0.83	1.66
1	108	4	432	0.67	0.67	2.68
1	108	6	648	0.55	0.55	3.3
1	108	8	864	0.47	0.47	3.76
1	108	10	1080	0.42	0.42	4.2

0.5	216	-20	-4320	0.39	0.195	-7.8
0.5	216	-18	-3888	0.44	0.22	-7.92
0.5	216	-16	-3456	0.51	0.255	-8.16
0.5	216	-14	-3024	0.6	0.3	-8.4
0.5	216	-12	-2592	0.74	0.37	-8.88
0.5	216	-10	-2160	0.95	0.475	-9.5
0.5	216	-8	-1728	1.33	0.665	-10.64
0.5	216	-6	-1296	2.22	1.11	-13.32
0.5	216	-4	-864	6.67	3.335	-26.68
0.5	216	-3.8	-820.8	8.33	4.165	-31.654

0.5	216	-3.6	-777.6	11.12	5.56	-40.032
0.5	216	-3.4	-734.4	16.72	8.36	-56.848
0.5	216	-3.3	-712.8	22.32	11.16	-73.656
0.5	216	-3.25	-702	26.81	13.405	-87.1325
0.5	216	-3.2	-691.2		0	0
0.5	216	-3	-648		0	0
0.5	216	-2.8	-604.8		0	0
0.5	216	-2.75	-594	26.65	13.325	-73.2875
0.5	216	-2.7	-583.2	22.21	11.105	-59.967
0.5	216	-2.6	-561.6	16.65	8.325	-43.29
0.5	216	-2.4	-518.4	11.09	5.545	-26.616
0.5	216	-2.2	-475.2	8.32	4.16	-18.304
0.5	216	-2	-432	6.65	3.325	-13.3
0.5	216	0	0	2.22	1.11	0
0.5	216	2	432	1.33	0.665	2.66
0.5	216	4	864	0.95	0.475	3.8
0.5	216	6	1296	0.74	0.37	4.44
0.5	216	8	1728	0.6	0.3	4.8
0.5	216	10	2160	0.51	0.255	5.1